419
1

SPUTTERING OF CdS THIN FILMS BY HEAVY ION BOMBARDMENT

Sputtering of CdS Thin Films by Heavy Ion Bombardment

by

NALIN R. PARIKH, M.Sc. (Physics)

PART A: ON-CAMPUS PROJECT*

A Report
Submitted to the School of Graduate
Studies in Partial Fulfilment of the Requirements
for the Degree
Master of Engineering

Department of Engineering Physics
McMaster University
Hamilton, Ontario, Canada

April, 1980

*One of two Project Reports: The other part is designated
Part B: OFF-CAMPUS PROJECT

MASTER OF ENGINEERING (1980) — McMASTER UNIVERSITY

Department of Engineering Physics — Hamilton, Ontario

TITLE: Sputtering of CdS Thin Films by Heavy Ion Bombardment

AUTHOR: Nalin R. Parikh, M.Sc. (Gujarat University, India)

SUPERVISOR: On-Campus: Dr. D. A. Thompson,
McMaster University

Off-Campus: Dr. R. A. Clarke,
Garrett Mfg. Ltd.
Toronto, Ontario

NUMBER OF PAGES: ix, 60

Abstract:

This report presents a study of the sputtering of vacuum deposited thin films of cadmium sulphide on a (111) face of single crystal silicon by Rutherford backscattering (RBS) technique. Cadmium was found to be preferentially sputtered when bombarded to high fluences of 80 kV Bi^+ while no significant preferential sputtering was observed in the case of 40 kV Ar^+ bombardment.

The structural study by reflection high energy electron diffraction (RHEED) revealed that the films grew epitaxially in the wurtzite structure. The epitaxial relations are (00.1) CdS||(111) Si with [10.0]||[110] Si.

Scanning electron microscope (SEM) microphotographs showed smooth surface features with a large grain size (surface grain size was ∿ 83 nm) for a film of about 60 nm thickness.

The basic structure did not change with highest fluences of Bi^+ (5×10^{16} ions/cm^2) and Ar^+ (6.7×10^{16} ions/cm^2). He^+ beam channeling was done for unbombarded and bombarded CdS films. It was found that the critical angle of channeling for cadmium increased for bombarded samples while for sulfur the statistics were too poor for any conclusion.

Saturation fluences for bismuth and argon retention were observed and are compared with calculated values.

ACKNOWLEDGEMENTS

I wish to thank my supervisor, Dr. D. A. Thompson, for his continuous support and guidance throughout the course of this work.

I also wish to thank Dr. J.A. Davies and Dr. G.R. Piercy for useful discussions during the course of this work. I would like to thank T. Vanderwel for depositing thin films of CdS.

I would like to thank my colleagues, especially D. Stevanovic and R. Newcombe for their unfailing help throughout this work and for proofreading the manuscript.

Finally, I am indebted to the Canadian International Development Agency and Brazilian Ministry of Industry and Commerce for supporting my study at McMaster.

INDEX

PAGE NO.

1. INTRODUCTION
   1.1 General 1
   1.2 Crystal structure 3
   1.3 Crystal binding 3
   1.4 Threshold displacement for Cd and S in CdS 4
   1.5 Important physical, electrical and thermo-dynamical properties of CdS 5
2. THEORY
   2.1 Bombardment induced structural changes 7
   2.2 Preferential sputtering of compounds 8
   2.3 Prediction of preferential sputtering of CdS by considering different effects 13
   2.4 Theoretical aspects of the experimental technique 15
      2.4.1 Rutherford backscattering technique 16
      2.4.2 Light particle channeling 18
   2.5 Trapping of the implanted atoms 19
3. EXPERIMENTAL
   3.1 Sample preparation 23
   3.2 Study of structure and morphology 23
   3.3 Ion implantation and RBS facilities 24
   3.4 Selection of ion species 25
   3.5 Target analysis 26
   3.6 Error estimation 27

PAGE NO.

4. RESULTS
4.1 Thickness calculation and channeling results 28
4.2 Bombardment induced structure and morphology changes of CdS thin films 29
4.2.1 Structure and morphology before bombardment 29
4.2.2 Structure and morphology after 5×10^{16} ions/cm^2 of 80 keV Bi^+ 32
4.2.3 Structure and morphology after 6.7×10^{16} ions/cm^2 of 40 keV Ar^+ 32
4.3 Sputtering of CdS thin films 32
4.3.1 80 keV Bi^+ bombardment of CdS 32
4.3.2 40 keV Ar^+ bombardment of CdS 33
4.4 Trapping of implanted ions 34
4.4.1 Trapping of Bi atoms 35
4.4.2 Trapping of Ar atoms 36
5. DISCUSSION
5.1 Channeling 37
5.2 Bombardment induced structure and morphology changes 37
5.3 Sputtering of CdS thin films 38
5.4 Trapping of implanted ions 40
6. CONCLUSIONS 41
7. REFERENCES 57

FIGURE CAPTIONS | PAGE NO.

		PAGE NO.
Fig. 1	Crystal structure of CdS	42
Fig. 2	RBS spectra after various fluences of Bi^+	43
Fig. 3	Schematic of McMaster on-line RBS and ion implantation facility	44
Fig. 4	A schematic of target chamber	45
Fig. 5	Backscattering yield versus tilt angle for Si, Cd, and S (unbombarded sample)	46
Fig. 6	Backscattering yield versus tilt angle for cadmium before and after bismuth and argon bombardment	47
Fig. 7	A RHEED pattern from an unbombarded CdS thin film	48
Fig. 8	A theoretical pattern corresponding to fig. 7	48
Fig. 9	An SEM microphotograph of an unbombarded CdS film	49
Fig. 10	A RHEED pattern from a Bi^+ bombarded CdS film	50
Fig. 11	An SEM microphotograph of a Bi^+ bombarded CdS film	50
Fig. 12	A RHEED pattern from an Ar^+ bombarded CdS film	51
Fig. 13	An SEM microphotograph of an Ar^+ bombarded CdS film	51
Fig. 14	Plot of areal density of Cd and S retained versus Bi^+ fluence	52
Fig. 15	Plot of percent of Cd excess w.r.t. stoichiometric compound versus Bi^+ fluence	52
Fig. 16	Plot of areal density of Cd and S retained versus Ar^+ fluence (sample at 40°K)	53
Fig. 17	Plot of percent of Cd excess w.r.t. stoichiometric compound versus Ar^+ fluence	53

		PAGE NO.
Fig. 18	Plot of areal density of Cd and S retained versus Ar^+ fluence (sample at 298°K)	54
Fig. 19	Plot of percent cadmium excess w.r.t. stiochiometric compound versus Ar^+ fluence	54
Fig. 20	Plot of trapped Bi atoms versus Bi^+ fluence	55
Fig. 21	Plot of trapped Ar atoms versus Ar^+ fluence (sample at 40°K)	56
Fig. 22	Plot of trapped Ar atoms versus Ar^+ fluence (sample at 298°K)	56

1: INTRODUCTION:

1.1 General:

Cadmium sulphide is a member of the group of semiconductors formed from elements in groups II and VI of the periodic table. In common with other members of the group, it has a wide band gap (2.42 eV) which makes it a promising material for the construction of electroluminescent devices with radiation emission in the blue and green positions of the visible spectrum. Unfortunately, CdS is normally either n-type or insulating, and attempts to produce p-type material by conventional doping methods have not been successful. This failure to type convert is attributed to a self-compensation effect which occurs at high temperatures and it is postulated that acceptor action is annulled by sulfur vacancies, which act as donors[1]. The doping of CdS by diffusion is also severely restricted due to the fact that dissociation of the compound occurs at relatively low temperature (> 450°C). It is for these reasons that the ion implantation technique has been used in attempts [2,3] to type convert CdS. Ion implantation is a non-equilibrium process and can be performed at any desired temperature.

The process of ion implantation involves directing a beam of energetic ions into a target material. The ions penetrate the surface of the target by virtue of their kinetic energy and are said to have been implanted. The penetration of the ions is a function of ion energy, the atomic masses of the incident

ions and the target, and, if a target is a single crystal, its orientation with respect to the incident beam direction. Using this technique it is possible to modify the near surface composition of a material in a controlled manner by selecting ions of any desired species and energy. An obvious application of this technique is to the doping of semiconductors, whose electrical characteristics can be controlled by the presence of small concentrations of various impurities; in fact, much of the early research work involved investigation of the properties of ion implanted Si[4]. Recently an application of this technique to metallurgy[5] has involved the production of alloys whose composition is not limited by ordinary solubility considerations[6] but is limited by a phenomena called sputtering, which is discussed below.

A serious disadvantage of this technique, however, arises from the dissipation of the kinetic energy of an energetic ion during implantation. In single crystal targets, this can cause extensive disruption of the crystal structure; i.e. radiation damage. At the surface, this radiation damage will cause surface atoms to be ejected from the target. This is known as sputtering. It is measured in terms of a sputtering coefficient, S, which is the ratio of the number of atoms ejected to the number of incident ions. In addition to the energy deposition, factors governing the sputtering yield are the target material, the target temperature and the angle of incidence. When a multi-elemental solid is bombarded with ions,

the surface region will be modified both as a result of the radiation damage and from an altered composition caused by different sputtering rates (called preferential sputtering) for different elements[7,8]. Composition changes by preferential sputtering have been studied in detail both for alloys[9,10] and oxides[8,11,12] while very little work has been done in case of compound semiconductors. Liau et al[10] have studied composition changes in single crystal InP and GaP and vacuum evaporated GeSi thin films.

1.2 Crystal Structure

Cadmium sulphide is a member of II-VI compounds which crystallizes either in the hexagonal wurtzite or the cubic zincblende structure. The hexagonal form is stable between 300°K and 1200°K, whereas the zincblende structure reverts to the hexagonal form at temperatures above 400°K. Fig. 1 shows the arrangement of cadmium and sulfur atoms in the hexagonal and cubic structures. Thin film CdS has been reported to grow in both structural forms depending upon the growth conditions: substrate structure and the plane on which it is grown. Data on the epitaxial growth of various materials on different single crystal substrates have been compiled by Matthews[13].

1.3 Crystal Binding

A cadmium atom has two s^2 electrons in its outer shell, and sulphur has six s^2p^4 electrons. Cadmium because of its high ionization potential, shares its s^2 electrons with the

neighbouring sulfur atoms instead of becoming fully ionized, producing four bonds directed towards the apices of a regular tetrahedron.

Thus, in cadmium sulphide, the bonding is partly ionic (0.74) and partly covalent, and the compound exhibits properties typical of both types of bonding.

1.4 Threshold displacement for Cd and S in CdS

Displacement of an atom from its lattice site by electron bombardment offers a unique and controllable means of producing isolated vacancy interstitial pairs of the host atoms of a crystal. For CdS where the atomic weights of the constituents are greatly different, it should be possible to observe two distinct thresholds for displacements, one at a lower energy representing displacement of the sulfur atoms and another at a higher energy representing displacement of cadmium atoms.

Kulp and Kelly[14] have observed a threshold for displacement in CdS for 115 keV electrons. This represents the transfer of a maximum energy of 8.7 eV to a sulfur atom. Bombardment by electrons above this energy produces two fluorescence bands at liquid nitrogen temperature: one band at 720 nm is attributed by these authors to the presence of sulfur vacancies; the other, green edge emission, to the presence of sulfur interstitial.

A threshold for the production of two fluorescence bands in CdS under electron bombardment at liquid nitrogen tem-

perature has been observed at 290 keV by Kulp[15]. This corresponds to a maximum energy transfer of 7.3 eV to the cadmium atom. The fluorescence bands produced are at about 605 nm and 1.03 μ which are believed to be due to Cd interstitial and Cd vacancies respectively.

Thus it appears that the cadmium atom is more weakly bound than the sulfur atom.

1.5 Important physical, electrical and thermodynamic properties of CdS

In table I important physical[16], electrical[16] and thermodynamic[17] properties of single crystal cadmium sulphide are listed.

TABLE I

Property	CdS
Structure	Wurtzite
Chemical binding	Mixed co-valent-ionic
Degree of ionicity	0.74
Melting point	1750°C
Molecular weight	144.42
Molecular density	4.05×10^{22} molecules$\cdot$cm^{-3}
Solid density	4.82 gm$\cdot$cms^{-3}
Band gap	2.425 eV
Dielectric constant*	8.28 - 8.64
Refractive index*	2.311 - 2.597
Thermal conductivity	0.2 w/°K-cm
Heat of atomization	57.0 K cal/g. atom
Heat of formation	38.0 K cal/mole at 298°K
Heat capacity at constant volume	7.8 (123°K), 13.8 (323°K) cal/mole×deg.
Heat of sublimation	51.0 K cal/mole

*Orientation dependent

2. THEORY

2.1 Bombardment induced structural changes

When an incident ion slows down and comes to rest it has violent collisions with some lattice atoms, displacing them from their lattice sites and finally producing a damaged condition which may or may not include a change in the structure of the bombarded solid.

At low ion fluence ($\lesssim 10^{13}$ ions/cm^2) one mainly concentrates on the formation of individual point defects as well as defect clusters. At intermediate fluence ($\sim 10^{13} - 10^{16}$ ions/cm^2) the damage includes amorphization, crystallization and stoichiometry changes depending on the solid, while at high fluence ($\gtrsim 10^{17}$ ions/cm^2) these three categories continue to be important and at the same time surface topographical alterations such as cones, pyramids, grooves and steps appear.

Naguib and Kelly[18] developed criteria for predicting amorphization, crystallization and stoichiometric changes in specimens for medium and high fluences of energetic ions. Whether the bombarded specimen will amorphize or crystallize is explained in terms of either a temperature ratio criterion, T_c/T_m (where T_c is temperature of crystallization and T_m is the temperature of melting) or a bond type criterion. The temperature ratio criterion is based on a model involving thermal spikes and states that amorphization occurs whenever the ratio exceeds 0.30. The bond type criterion is of a more or less empirical origin; it states that amorphization occurs

whenever the ionicity is ≤ 0.47. (Ionicity of CdS $\simeq 0.74$.)

According to the above criteria cadmium sulphide should not amorphize under ion bombardment.

2.2 Preferential sputtering of compounds

Basically two interesting phenomena may be observed when a homogeneous two component system is irradiated by energetic ions viz. preferential or non-stiochiometric sputtering and radiation induced composition gradients in the target. Preferential sputtering does not necessarily (although usually) lead to concentration gradients, but other radiation induced mechanisms such as enhanced thermal diffusion, recoil implantation, etc. may be responsible for concentration gradients near the irradiated surface.

Sigmund[19] has developed a comprehensive sputtering theory based on radiation damage theory which gives good agreement with experimental observations. For ions which are incident normally upon a target material, Sigmund's theory predicts that the sputtering yield at an ion energy E is given by

$$S(E) = \frac{k}{U_0} \cdot Sn(E, Z_1, Z_2) \cdot \alpha\left(\frac{M_2}{M_1}\right) \qquad 2.1$$

where k is a constant

U_0 is the surface binding energy for the target atoms

Sn is the nuclear stopping power, and

α is a function depending on the mass ratio $\left(\frac{M_2}{M_1}\right)$ of the target atoms and bombarding particles.

According to this model, two different mechanisms lead to preferential sputtering of oxides, alloys, halides and semiconductor compounds, viz. surface binding effects and mass difference effects.

The binding energy effect is illustrated by the much studied Cu-Ni systems, where the masses are so close that effects of their difference may be neglected. According to Ono et al[20] the change in composition may be interpreted by assuming $S_{Cu}/S_{Ni} = U_{Ni}/U_{Cu}$ for all bulk compositions of the system. S_{Cu} and S_{Ni} are the sputtering yields of copper and nickel respectively.

Mass difference effects act via different mechanism at low and high energies. At low energies (close to the threshold displacement energy) the projectile to the target mass ratio becomes an important factor. Approximately equal masses favor an efficient energy transfer, hence if the projectile mass is close to that of one target component but not to the other, sputtering of the former element is enhanced. A double collision is necessary to invert the momentum of the primary knock-on to give backsputtering. A light target component may have its momentum inverted by colliding with a heavy component, but not vice versa. Hence the sputtering of the light component is favoured[21].

At higher energies, sputtering occurs through a collision cascade mechanism. Light and heavy components are predicted to be sputtered with different energy spectra and with

a preferential sputtering of the light component[22]. Other theories[23] start by assuming energy equipartition among the displaced atoms, an assumption that is at variance with the result of the linear theory. For heavy projectiles and energies well up in the keV range, energy spikes develop, producing pronounced nonlinear effects[24]. Here the equipartition assumption may be a good one, and even more pronounced preferential sputtering of the light component is predicted.

Kelly[8] showed that mass effects cause the lighter atoms to sputter faster proportionately, than the heavier atoms. He extended the theory of recoil implantation[11] to deal with the atoms sputtered from the surface by the action of the low-order recoil atoms.

The final result of this model is

$$\frac{S_A}{S_B} = \frac{x_A \cdot M_B^{1/3} \cdot (M_1+M_B)^{2/3}}{x_B M_B^{1/3} (M_1+M_A)^{2/3}} \left(\frac{M_1^{2/3}+M_B^{2/3}}{M_3^{2/3}+M_B^{2/3}}\right)^{2/3} \times \left(\frac{M_3^{2/3}+M_A^{2/3}}{M_1^{2/3}+M_B^{2/3}}\right)^{2/3} \times \frac{j(M_3/M_A)}{j(M_3/M_B)} \qquad (2.2)$$

where M_1 is the atomic mass of the incident particle

M_A, M_B are the atomic masses of the constituent elements A and B respectively

M_3 is an average atomic mass in the unsputtered bulk of the target

x_a, x_B are the atomic fraction of atoms of A and B

and $j(M_3/M_A)$ and $j(M_3/M_B)$ are functions of the recoil atom distribution:

$$j(M_3/M_A) \simeq (2h)^{1/2} \int dw\, w^{-1/3} \cdot \mathrm{ierfc}\{fw/(2h)^{1/2}\}$$

where: $(2h)^{1/2} = \frac{\langle y \rangle N_3 c}{T_2^{2/3}} \cdot \sqrt{2}$

N_3 is the average number density of atoms in the target.

c is a constant

$\langle y \rangle$ is the average distance an incident ion is deflected from its initial line of motion

T_2 is the energy transferred, in a low order recoil, from the incident particle of energy E and mass M_1 to the target particle of mass M_2

$$T_2 = E \cdot \frac{4 \cdot M_1 M_2}{(M_1+M_2)^2} \cdot \omega$$

where $\omega = \sin^2(\theta/2)$

and θ is the angle between the line of motion of the target particle and the initial line of motion of the incident particle in center of mass coordinate.

$$f = \langle x \rangle N_3 c / T_2^{2/3}$$

where $\langle x \rangle$ is the mean projected range of the ions in the target.

An alternative treatment of the problem was undertaken by Haff[26]. He assumed that the extracted beam energy is quickly equilibrated among all cascade members, independent of their mass, and that displaced atoms in the cascade undergo a diffusion-like motion before they come to rest.

He concluded that the number of atoms lost due to sput-

tering is proportional to $(Dt)^2$, the diffusion distance, and thence proportional to $v^{1/2}$ and to $M^{-1/4}$

where D is the pseudo-diffusion constant

v is the average velocity of the recoiling atoms

and t is the pseudo-diffusion time.

Haff finally concluded that the loss ratio for a target consisting of A and B is

$$\frac{\text{loss of A}}{\text{loss of B}} = (M_B/M_A)^{1/4} . \tag{2.3}$$

In his recent review article Kelly[25] discusses the problem of whether the mass or chemical bonding of the constituent elements is more important to bombardment induced compositional changes. He concludes that chemical binding is more important than mass based upon many oxides and alloys studied. There are other effects that deplete the surface of a particular component which are mentioned below.

Recently thermal segregation has been discussed by Brongersma et al[26]. From their analysis, it appears that elements which thermally segregate at the surface will have the lowest binding energy and hence be preferentially sputtered. Such effects will cause even larger transients in surface composition than those due to preferential sputtering.

Recoil implantation from the surface will deplete the surface of its lighter component[8] and hence may easily be con-

fused with preferential sputtering if only an altered layer is studied.

Radiation enhanced segregation of misfit solute atoms may give rise to very striking surface composition changes during high energy irradiation, as demonstrated by Rehn et al[27]. If one of the components transfers from the solid phase to the gaseous phase at the temperature investigated, it diffuses faster and precipitates (or is released) at the surface. In this case this component will be preferentially sputtered.

2.3 Prediction of preferential sputtering of CdS by considering different effects.

(i) Mass difference effect: $\frac{M_{Cd}}{M_S} \simeq 3.5$

According to Kelly's formula[25], eqn. 2.2,

For $\frac{M_A}{M_B} = 3$, $\frac{S_A}{S_B} = 0.31$

while according to Haff's formula[26], eqn. 2.3,

for $\frac{M_A}{M_B} = 3$, $\frac{S_A}{S_B} = 0.76$.

Thus the mass difference consideration predicts the preferential sputtering of the lighter component, i.e. sulfur.

(ii) Binding energy effect:

The threshold energy for displacement of a Cd atom = 7.3 eV

The threshold energy for displacement of a S atom = 8.7 eV.

The binding energy consideration predicts the preferential

sputtering of the loosely bound component, i.e. cadmium. A rough estimate of the amount of preferential sputtering is predicted on the basis of Sigmund's theory discussed earlier.

$$\frac{S_A}{S_B} = \frac{U_B}{U_A} \quad ; \quad \frac{S_{Cd}}{S_S} = \frac{8.7}{7.3} \simeq 1.2 \ .$$

Here preferential sputtering of cadmium is predicted by almost 20% for stoichiometric CdS.

(iii) Thermal effects:

The thermal effects are significant only if

(a) the target is sitting at or near the temperature of decomposition of CdS (450°C);

(b) the current density of the ion beam is sufficient to raise the temperature, locally, to $\gtrsim$ 450°; or

(c) a high density cascade creates a thermal spike.

In this work, (a) and (b) do not apply: the target was always at or below room temperature.

(iv) Recoil implantation from the surface will deplete the surface of its light component[8].

(v) Internal precipitation effect:

For the temperature investigated, neither cadmium nor sulfur exist in a molecular gaseous form and should not precipitate as such.

Kelly and Naguib[18] have proposed a theory of preferential sputtering which predicts equilibrium ratios for compound

compositions in terms of the minimisation of the combined heats of atomisation of the components of the compound (assuming that heat of atomisation is approximately equal to the binding energy of the components).

A calculation based upon this theory for the equilibrium composition of sputtered cadmium sulphide predicts a compound with sulfur excess, i.e. preferential sputtering of cadmium.

2.4 Theoretical aspects of the experimental technique

The change in stoichiometry due to preferential sputtering will result in the composition changing until the target reaches a steady-state after which it sputters stoichiometrically, i.e. such that the ratio of the sputtering yields equals the ratio of atoms in the bulk. This must be so, to conserve mass. For preferential sputtering restricted to the near surface region, this steady state condition will be reached rapidly. However, if atoms can diffuse to or from the surface at an appreciable rate, the region of non-stoichiometry will be extended over the ion range. Therefore it will take longer to reach a steady-state. If the sputtering rate is low enough, and diffusion is fast enough, the steady-state sputtering may be non-stoichiometric.

Preferential sputtering may be investigated experimentally by studying changes in surface composition during irradiation, by the development of a composition profile through an altered layer, or through deviations of the composition of

the sputtered flux from that of the bulk target. In the present work, sputtering of CdS was studied by measuring areal density (atoms/cm^2) of retained film by Rutherford backscattering (RBS) technique.

A brief description of the RBS technique follows.

2.4.1 Rutherford Backscattering (RBS) technique

In a typical backscattering experiment, a beam of high energy (1-2 MeV) protons or helium ions is incident upon a target material which is to be investigated. The ions interact with the target atoms through a series of both elastic and inelastic collisions. The elastic collisions involve nuclear interactions, while inelastic collisions impart energy to the electrons of the target material. The relative frequency of elastic and inelastic collisions depends upon the energy of the incident ions, atomic number and atomic masses of the incident ions and the target material. For the light particles, like protons and helium with 1-2 MeV energies, an elastic collision involves a close nuclear encounter, and is dominated by the Coulombic repulsion between nuclei, a situation which can be described in terms of the Rutherford scattering law[28].

The differential scattering cross-section in center of mass coordinates is given by

$$\frac{d\sigma}{d\omega} = 1.296\times10^{-25} \left(\frac{Z_1 Z_2}{E_0}\right)^2 \left(\frac{M_1+M_2}{M_2}\right)^2 \sin^{-4}\left(\frac{\theta_s}{2}\right) \text{ mm}^2/\text{steridian} \tag{2.4}$$

where E_0 is the energy of the incident ions in MeV

Z_1 and Z_2 are the atomic numbers of the incident ion and the struck target atom respectively

M_1 and M_2 are the atomic masses of the incident ion and the struck target atom respectively

θ_s is the scattering angle in center-of-mass coordinates measured in cm^2/steradian

and $$\theta_s = \theta_L + \sin^{-1}\left(\frac{M_1}{M_2} \sin\theta_L\right)$$

where θ_L is the scattering angle in laboratory coordinates.

A small fraction of the incident ions will undergo elastic collisions while the majority will lose energy inelastically and eventually come to rest at some depth inside the target.

The total number of backscattered ions received by a suitably placed detector is given by

$$\text{Yield} = (N\Delta x)\, n \left(\frac{d\sigma}{d\omega}\right) \Delta\omega \tag{2.5}$$

where the $N\Delta x$ is the areal density of the target atoms (atoms/cm^2)

n is the fluence of the incident ions (ions/cm^2)

and $\Delta\omega$ is the solid angle subtended by the detector in steradians.

The energy of the ions scattered from the surface is given by

$$E = K^2 E_0 = \left(\frac{M_1 \cos\theta_L + M_2}{M_1 + M_2}\right)^2 E_0 \qquad (2.6)$$

Therefore one can identify a target material by analysing the energy spectrum of the backscattered particles. A typical RBS spectra of thin film CdS on silicon substrate is shown in fig. 2.

Ions which penetrate the surface will steadily lose their energy through electronic excitation and ionization. If the rate of energy loss as a function of energy is known, the energy spectrum of the backscattered ions can be converted to a depth profile of the target atoms. Applications of ion-implantation technique are discussed in reference 29.

2.4.2 Light particle channeling

When a fast moving charged particle enters a crystal within a small critical angle of a close packed atomic row (axial channeling) or plane (planar channeling), it becomes channeled i.e. it becomes steered by successive gentle collisions, and is thereby prevented from having violent collisions with individual lattice atoms. In other words as long as it remains channeled, a particle will not undergo elastic scattering with atoms in the rows or planes. Hence, the observed RBS yield will be reduced drastically ($\sim$ 98 - 99%) from that

obtained on bombarding the crystal along a random (non-aligned) direction. An excellent review on channeling and its applications is written by Gemmell[30]

The critical angle is given by

$$\psi_{crit.} = \left\{ \frac{2Z_1Z_2e^2}{E_0d} \right\}^{1/2} \qquad (2.7)$$

where d is the distance between adjacent atoms along either rows or planes

e is the electronic charge.

The ratio of the backscattered yield of the aligned spectrum to the random spectrum χ_{min} is not calculated here because of unknown parameters like defect concentration in thin films and thermal vibrational amplitudes.

2.5 Trapping of the implanted atoms

At very low implantation fluence where the atomic concentration of implanted atoms is so low that even in thermal equilibrium at elevated temperature the solubility limit is orders of magnitude greater, the implanted atoms will remain as isolated impurity atoms within the host lattice. These atoms can occupy either substitutional or interstitial sites depending on which corresponds to the lowest free energy state, which in turn depends on parameters such as the size and electronic configuration of the atoms. In practice, the majority of the implanted atoms come to rest in an environment where initially both lattice interstitial and vacancies are plentiful; and in the case of semiconductors, sometimes but not necessarily within zones of a different crystalline

state which may be produced by the ion bombardment. Calcu-ations suggest that within a random collision cascade the incident ion has a high probability of finally coming to rest as a consequence of a replacement collision and therefore occupying a substitutional site. If the surrounding lattice interstitials and vacancies produced by the irradiation are mobile, this atom may subsequently move by any one or a combination of the following mechanisms: a) Vacancy exchange, b) pinning or trapping to a lattice interstitial, c) thermal activation into a free interstitial configuration leaving a vacancy, d) in some cases direct replacement by a lattice interstitial. In general, free interstitials have low activation energies for migration and rapidly move through the lattice until they trap at defects or surfaces or cluster with other interstitials.

The trapping of the implanted atoms is described in terms of a trapping or collection coefficient (η) which is the ratio of the density of trapped atoms n_T to the implant ion fluence n_I. η is measured from the slope dn_T/dn_I as $n_I \to 0$. Typically, measurements[31] reveal that for low ion fluence, η remains relatively constant but as fluence increases the apparent trapping coefficient falls toward zero and a saturation of implanted atoms occurs, i.e. a steady state is reached at which point for each atom implanted one is ejected from the surface. The steady state results when all

available traps become filled and by simultaneous evolution processes such as sputtering processes of either host atoms or direct sputtering of impurity atoms. Electronically stimulated emission processes are also possible in semiconductors and insulators.

Carter and coworkers[32] proposed a simple model of ion-collection in a target which is based on the following assumption:

(i) There is no range shortening due to the collected ions in the target,

(ii) that a constant sputtering coefficient for the ion-target combination is operative throughout the process,

(iii) that the range distribution is not broadened due to knock-on of implanted atoms by subsequent ions, and

(iv) that the dopant atoms do not escape the target at a rate different to that of sputtering of target atoms.

These assumptions imply that as bombardment continues the two processes of implanted atom collection and sputtering proceed simultaneously in such a way that initially the probability of the ion stopping is of a Gaussian form with a mean range at a depth R_p relative to the initial surface. As bombardment proceeds this penetration profile is retained relative to the instantaneous surface which recedes from the initial position due to sputtering, and previously implanted atoms are released from the target as the instantaneous surface crosses the regions

of implant location. There is thus a continuous competition between implant collection and implant removal which eventually leads to a collection saturation.

According to this theory saturation occurs when the incident ion fluence has been sufficient to sputter a depth equal to a maximum ion range, which as a first approximation might be taken as the range where the ion stopping probability is 10 per cent of that at the most probable range R_p. This occurs at a distance of the order of the $R_p+2\Delta R_p$ where ΔR_p is the standard deviation of the Gaussian range profile and occurs at a value of fluence of

$$n(R_p+2\Delta R_p)/S \qquad (2.8)$$

where n is the target atom or molecular density and S is the target sputtering coefficient.

R_p and ΔR_p for 80 keV Bi^+ and 40 keV Ar^+ in CdS were calculated from Winterbon[33] calculations, which are as follows:

	R_p	ΔR_p
For 80 keV Bi^+	21.9 nm	3.0 nm
For 40 keV Ar^+	29.8 nm	10.4 nm

Taking $n = 4.05\times10^{22}$ CdS molecules$\cdot$cm^{-3} eqn. (2.8) gives

saturation fluence for Bi occurs at $\frac{1.13\times10^{17}}{S}$ ions/cm^2, while

saturation fluences for Ar occurs at $\frac{2.05\times10^{17}}{S}$ ions/cm^2

where S is the sputtering yield in CdS $\frac{\text{molecules}}{\text{ion}}$. This assumes no preferential sputtering.

3. EXPERIMENTAL

3.1 Sample preparation

Thin films of cadmium sulphide were prepared at Garrett Mfg. Ltd., Toronto, using the hot wall technique[34] to ensure nearly stoichiometric films. The major parameters of evaporation are as given below

Substrate temperature	230°C
Source temperature	850 - 900°C
Wall temperature	200°C
Deposition rate	2.5 nm/sec.

A detailed explanation of the experimental set-up and deposition procedure is given in reference 35.

A silicon single crystal ((111) surface) was used as a substrate material because it has a lower Z than sulfur and cadmium. As such, the Si part of the RBS spectrum is separated from that due to the thin film of CdS, which appeared as two resolved peaks corresponding to Cd and S. Films of about 60 nm thickness were normally used for this work.

3.2 Study of structure and surface morphology

The effects of ion bombardment on structure and morphology were studied by reflection high energy electron diffraction (RHEED) in an electron microscope (Philips Model EM 300), and by scanning electron microscope (SEM) (Cambridge Stereoscan type 96113).

For the RHEED study, an electron energy of 40 keV was

employed while SEM work was carried out at 20 keV. SEM micrographs were taken at 45° tilted angle to get the best contrast.

3.3 Ion implantation and RBS facilities

The samples were ion implanted and RBS analysed in situ, in the McMaster University Accelerator laboratory, solid state facility. A detailed description of this facility is given in ref. 36.

Fig. 3 shows the schematic diagram of the coupled system used in the present work. A He^+ beam of MeV energy from the Van de Graaff accelerator is passed through an analysing magnet, and through two 0.75 mm diameter apertures separated by 0.96 m to ensure good collimation (full angle $\sim$ 0.07°). The backscattered ions from the target were detected by a standard silicon surface barrier detector, (FWHM 16 keV) mounted at 150° to the beam direction. The output from the detector after being amplified was fed to a pulse height analyser, which gave the energy spectrum of the backscattered particles.

The 150 kV ion implantation accelerator is a Texas Nuclear Corporation model 9509 Cockroft-Walton neutron generator that has been modified to accommodate a Danfysik 911 A Universal ion source. During implantation, the collimating apertures were replaced by 2 mm and 4 mm diameter apertures, the former being nearest the analysing magnet. For implantation the apertures were off axis so that those ions which were neutralized in a charge exchange collision with residual gas atoms

in the beam line could not reach the target. Between these apertures were two pairs of electrostatic beam sweep plates to allow for horizontal and vertical sweeping of the beam. The uniform area ($\sim 0.42\ cm^2$) on the target is defined by electrostatically sweeping the beam across the 4 mm aperture. A schematic of target chamber geometry is shown in fig. 4. The sample was mounted on a goniometer so that it could be rotated about an axis parallel to the incident beam direction and tilted (+45° to -20°) with respect to incident beam direction. The target could be cooled to about 40°K by a cryocooler.

The target chamber pressure without the cryocooler operating was $\sim 3\times10^{-6}$ Torr while with the cryocooler on, the pressure surrounding the target was $< 10^{-9}$ Torr.

In this work RBS analysis was done with 2 MeV He^+, with a beam current of 2 nA which gave a low dead time (< 2%) and a small amount of pulse pile up.

3.4 Selection of ion species

Bismuth and argon ions were selected for implantation for the following reasons. First bismuth, being a member of group V of the periodic table is a well studied acceptor dopant. Also, since bismuth is heavier than cadmium, it falls on the higher energy side of the RBS spectrum.

Argon was selected because it is a member of the group of inert gases and at the same time its atomic mass is between Cd and S..

The energies of the ion species were selected arbitrarily. In the case of argon implantation the specimens were bombarded at two different temperatures to see whether this would have any influence on the sputtering results. Three sets of experiments were performed:

	Bombarded species	Temperature of the Specimen
Set I	80 keV Bi^+	40°K
Set II	40 keV Ar^+	40°K
Set III	40 keV Ar^+	298°K

3.5 Target Analysis

During the RBS analysis to determine the CdS thickness before and after bombardment the sample was continuously rotated in order to avoid channeling of He^+ ions through the film, while during the implantation the sample was tilted away from the channeling direction.

Channeling investigations of unimplanted and implanted cadmium sulphide samples were also carried out with respect to the <111> axis of silicon to check for CdS alignment. For unimplanted and implanted samples critical angles were found and aligned and random spectra were taken to calculate the relative minimum yield (χ_{min}).

3.6 Error estimation

Errors in calculation of areal densities of cadmium and sulfur were estimated to be about ± 4%. Following are factors which contributed to above estimation.

a) 0.5% error in measurement of incident energy (E_0)

b) 1.0% error in measurement of scattering angle (θ_L)

c) 2% error in measurement of solid angle sustended by detector ($\Delta\omega$)

d) Errors in measurement of yield (statistical error, max. 0.5%).

Errors in the calculation of implant ion fluences were due to errors in the measurements of implanted areas (about ± 5%) and errors in the measurements of ions implanted (current integration, max. 0.4%). When one considers the ratio of the areal densities of cadmium and sulfur, the relative error is very small (< 2%) which comes from the measurement of the yields of cadmium and sulfur (statistical error). Hence the results in terms of excess of one component can be given accurately to < 2%.

4. RESULTS

In this chapter the initial thin CdS films are analysed to determine the thickness and structural properties of the as produced film and changes due to bombardment. Surface erosion (sputtering) and compositional changes resulting from ion bombardment are determined as is the number of ions trapped in the film.

4.1 Thickness calculation and channeling results

4.1.1 Thicknesses of the unimplanted and implanted CdS films were calculated from the areal density assuming that the density of the CdS films is the same as the bulk material. An estimated error of ± 10% came from errors in measurement of areal density and nonstoichiometry in the film. The thickness results are given in Table II.

Table II

Set I	Thickness of unimplanted CdS 59 nm	Thickness after Bi^+ fluence of 5×10^{16} ions/cm^2 28 nm
Set II	Thickness of unimplanted CdS 93 nm	Thickness after Ar^+ fluence of 9.3×10^{16} ions/cm^2 45 nm
Set III	Thickness of unimplanted CdS 94 nm	Thickness after Ar^+ fluence of 6.7×10^{16} ions/cm^2 63 nm

4.1.2 Channeling

Unbombarded, argon bombarded (fluence of 6.7×10^{16} ions/cm^2) and bismuth bombarded (fluence of 5×10^{16} ions/cm^2) CdS films were studied using the channeling technique. A He^+ beam was aligned with respect to the Si<111> axis by monitoring the backscattering yield from Si while scanning (the sample) about the Si<111> axis. The backscattering yields of Si, Cd and S were measured and a plot of backscattered yield versus tilt angle was drawn for these elements. Fig. 5 shows a typical plot of an unbombarded sample. Half the critical angle ($\psi_{1/2}$) and χ_{min} for unbombarded, argon bombarded and bismuth bombarded samples are given in Table III.

In another plot (fig. 6) the backscattering yield versus tilt angle for cadmium is shown before and after bismuth and argon bombardment. Note that the critical angle for cadmium becomes larger after bombardment. Because of the poor statistics the critical angle for sulfur was not measured, however the dip which was observed clearly for the unbombarded sample was not clear. The critical angle for silicon was not changed by ion bombardment, as would have been expected. The χ_{min} for cadmium and sulfur did not change after bombardment while the silicon χ_{min} decreased because the part of the CdS film was sputtered off.

4.2 Bombardment induced structure and morphology changes of CdS thin films.

4.2.1 Structure and morphology before implantation

Figure 7 shows the RHEED pattern from an unbombarded CdS thin film, which consists of spots and faint arcs. A set

Table III

$\psi_{1/2}$ Calculated		Silicon	Cadmium	Sulfur
$\psi_{1/2}$ experimental	unbombarded	0.65°	0.65°	0.65°
	Bi^+ bombarded	0.65°	1.1°	*
	Ar^+ bombarded	0.65°	1.5°	*
χ_{min} for unbombarded sample		0.83±0.02	0.72	0.70
χ_{min} for Bi^+ bombarded sample		0.55	0.72	0.71
χ_{min} for Ar^+ bombarded sample		0.68	0.74	0.72

*Because of the poor statistics critical angles were not found.

of 00.0, 00.2, 10.2, 10.0* reflections forming a rectangle with sides in ratio of $\sqrt{3}:\sqrt{8/3}$ attests to the growth of the hexagonal wurtzite structure. The existence of the hexagonal phase is further substantiated by the observed sixfold repetition of the diffraction pattern on rotation of the specimen about the beam axis.

Reflections such as 00.1, 10.1 ... forbidden by the structure factor for the hexagonal system, are present. It is known[37] that these reflections result from double diffraction in the (10.0) section, i.e. when the electron beam is along a <11.0> direction.

The epitaxial relations are as given below:

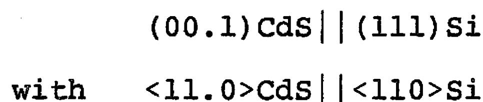

Lattice parameters of $a_0 = 4.13$ Å and $c_0 = 6.71$ Å were determined from the RHEED pattern which are in close agreement with the handbook values.

A theoretical pattern corresponding to fig. 7 is shown in fig. 8.

An SEM micrograph of unimplanted CdS is shown in fig. 9. The sample was tilted at 45° to the optical axis of the microscope. The micrograph shows a smooth surface with an average surface grain size around 83 nm, which is larger than the thickness of the film (60±6 nm).

---

*A standard crystallographic notation is used.

4.2.2 Structure and morphology after 5×10^{16} ions/cm^2 of 80 keV Bi^+

A RHEED pattern after 80 keV Bi^+ bombardment of total fluence of 5×10^{16} ions/cm^2 is shown in fig. 10. Note that the spots and faint arcs were replaced by short intense arcs. Although there was some radial arcing of the spot patterns, there was never any distinct evidence of a breakdown of the crystalline pattern to the diffuse rings which indicates that film is maintaining its crystalline structure.

The morphology of the film corresponding to the diffraction pattern of fig. 10 is shown in an SEM micrograph (Fig. 11). The SEM micrograph shows that the morphology of the film changed from a continuous, smooth, to a slightly rough surface. There may be a development of facets in the grains but on such a small scale that it is difficult to resolve at 17 K magnification.

4.2.3 Structure and morphology after 6.7×10^{16} ions/cm^2 of 40 keV Ar^+

A RHEED pattern after total fluence of 6.7×10^{16} ions/cm^2 of 40 keV Ar^+ is shown in fig. 12 which is very similar to an unbombarded specimen. A corresponding SEM micrograph of the RHEED pattern of fig. 12 shows no change in film morphology (fig. 13).

4.3 Sputtering of CdS thin films

4.3.1 80 keV Bi^+ bombardment of CdS

Fig. 2 shows some RBS spectra of a CdS film at different stages of a Bi^+ bombardment. From these spectra the areal

densities of retained Cd and S atoms were calculated using eqn. (2.5). Fig. 14 shows the areal density (atoms/cm^2) for cadmium and sulfur as a function of Bi^+ fluence. It can be seen that cadmium areal density decreases faster than sulfur areal density with increasing fluence of Bi, which indicates that Cd is being preferentially sputtered. The same results are plotted in fig. 15, which shows per cent excess of Cd, w.r.t. stiochiometric compound versus Bi^+ fluence. It is seen from this plot that the CdS films which were rich in Cd before implantation lost cadmium preferentially with increasing Bi^+ fluence. For total fluence of 5.0×10^{16} ions/cm^2 excess cadmium dropped from 22.4% to 12.2%. Absolute errors in density calculation were found to be less than ±5% while errors in percent excess was about ±2%. (Ref. sec. 3.6). The average sputtering yield from the fluence of 10^{15} ions/cm^2 to saturated fluence for sulfur was found to be 5.0±1.4 atoms/ion while for Cd it was 6.8±1.4 atoms/ion.

4.3.2 40 keV Ar^+ bombardment of CdS

a) Sample at 40°K

Fig. 16 shows the plot of areal density of Cd and S retained versus Ar^+ fluence. From this plot it can be noted that sulfur density is increasing marginally w.r.t. initial composition as Ar^+ fluence is increased. But the marginal increase in sulfur density is within the experimental errors and

no definite conclusion can be drawn from this result. This is further justified by the plot of percent excess of cadmium versus Ar^+ fluence which does not indicate any preferential sputtering (fig. 17).

b) Sample at room temperature (298°K)

There was no significant difference in the results obtained when the sample was at room temperature or at 40°K.

A plot of cadmium and sulfur retained versus Ar^+ fluence is shown in fig. 18, while fig. 19 shows the plot of percent excess Cd versus Ar^+ fluence. These plots, again, show that there is no preferential sputtering of any component.

At both temperatures the average sputtering yield between a fluence of 10^{15} ions/cm^2 and the saturated fluence was found to be equal to 1.5±0.3 atoms/ion for both cadmium and sulfur.

4.4 Trapping of implanted ions

A typical set of spectra obtained by 2 MeV He^+ scattering from a sample implanted with 80 keV Bi^+ can be seen in fig. 2, which shows the bismuth peak increasing in size with increasing fluence. The total number of bismuth atoms trapped was calculated by finding the number of counts under the peak and putting this value in equation (2.5).

Despite the reasonably separated peaks some overlap occurred between the bismuth and cadmium peaks. This affects the accuracy of measurement of the bismuth counts, particularly

at low fluence (< 10^{15} ions.cm^{-2}), where the low yield necessitates longer collection times to produce acceptable statistics.

In the same way, in the case of argon implantation, the peaks of argon and sulfur are overlapped even when analysing with a 2 MeV He^+ beam, which causes a large error in the measurement of the argon counts at low fluences.

4.4.1 Trapping of Bi atoms

Fig. 20 shows a plot of retained or trapped bismuth atoms as a function of Bi^+ fluence. The straight line represents a collection coefficient (η) of about one, i.e. the amount of bismuth trapped is equal to the amount of bismuth implanted.

The trapping of bismuth saturates for fluences of around 4×10^{16} ions.cm^{-2}. The total error in these measurements was estimated to be less than ± 6%. (Ref. sec. 3.6).

The saturation fluence for Bi^+ calculated from eqn. (2.8) is

$$\frac{1.13\times10^{17}}{S} = \frac{1.13\times10^{17}}{6\pm1.4} \simeq 2\times10^{16} \pm 0.3\times10^{16} \text{ ions.cm}^{-2}$$

where S = 6±1.4 molecules/ion.

The calculated saturation fluence is about one half that observed.

4.5.2 Trapping of Ar^+ atoms

Figs. 21 and 22 show the plots of trapped Ar atoms as a function of Ar^+ fluence, when the sample is at 40°K and at room temperature. The collection coefficient for both the temperatures is about 0.65, i.e. only 65% of the implanted Ar^+ ions are trapped in the sample (over the range of fluences 2×10^{15} to 3×10^{16} ions.cm^{-2}).

Saturation levels of $\sim 7\times10^{16}$ atms.cm^{-2} and $\sim 5\times10^{16}$ atoms.cm^{-2} were found for samples at 40°K and at room temperature respectively.

The saturation fluence calculated from eqn. (2.8) is

$$\frac{2.05\times10^{17}}{1.5\times0.3} = 1.4\times10^{17} \pm 0.20\times10^{17} \text{ ions.cm}^{-2} .$$

i.e. the calculated saturation fluence is $\gtrsim$ 2x the observed value.

5. DISCUSSION

5.1 Channeling

Channeling results showed that the critical angle for cadmium increased after ion bombardment and the RHEED study showed that the structure was epitaxial before bombardment and changed to one degree oriented polycrystalline. These results suggest that due to bombardment crystallites reoriented such that the critical angle became larger. There was ∿ 1° increase in the critical angle after Bi^+ bombardment suggesting that crystallites oriented by ∿ 1/2° on both sides of the channeling direction. Such a small tilting of the crystallites will not change the basic structure but will increase in the arc length which has been observed by RHEED pattern (fig. 10).

5.2 Bombardment induced structural changes

The cadmium sulphide thin films grown on Si(111) faces had the hexagonal wurtzite structure of CdS with $a_0 = 4.13$ Å and $C_0 = 6.71$ Å. They grew with their basal plane parallel to the (111) plane of Si and <11.0> directions parallel to the <110> directions of the Si single crystal. A similar growth on (111) faces of single crystal NaCl has been reported[38].

The basic crystal structure of CdS thin films did not change after 40 keV Ar^+ and 80 keV Bi^+ bombardment, to total fluences of 6.7×10^{16} ions/cm^2 and 5×10^{16} ions/cm^2 respectively. It is therefore concluded, at least in the present situation, that 80 keV Bi^+ and 40 keV Ar^+ bombardments do not produce

amorphous zones as is the case of Si[39], Ge and III-V semiconductors[36]. Similar results were observed by Govind and Fraikor[40], and Eldridge et al.[41] for 25 keV Bi^+ bombarded single crystal CdS to total fluences of up to 3×10^{16} ions/cm^2, using transmission electron microscopy (TEM) and high energy electron diffraction (HEED) studies respectively.

5.3 Sputtering of CdS thin films

In section (2.8) the different effects that could lead to preferential sputtering of either component of the binary compound were explained. The mass effect and the recoil implantation effect predict preferential sputtering of the lighter component, i.e. sulfur in CdS, while the binding energy effect predicts that the loosely bonded cadmium would be preferentially sputtered.

The results of Bi^+ bombarded CdS clearly show the preferential sputtering of cadmium. The cadmium excess dropped by about 10% ± 2% for a total fluence of 5×10^{16} ions/cm^2. Preferential sputtering of cadmium was also observed by Baxter[42] for 40 keV Bi^+ implanted single crystal of CdS. He found the specimens yielded an average of 13±5% sulfur excess for total fluence of 1×10^{16} ions/cm^2.

In the case of Ar^+ bombardment no significant preferential sputtering was observed. This is again in agreement with Baxter's results for the same energy.

The presence of excess cadmium in the unbombarded CdS

films was at first thought to be responsible for preferential sputtering of cadmium because either excess cadmium atoms have formed Cd clusters with Cd-Cd bonds which are much weaker compared to Cd-S bonds (Cd-Cd chemical bond strength is 2.7 KCal/mol while Cd-S chemical bond strength is 48 KCal/mol) or there are large numbers of sulfur vacancies in the films which leave some of the Cd bonds dangling.

If this is the case then we should have observed the preferential sputtering of cadmium with argon bombardment which is not true. However the above results can be explained qualitatively if we consider that the energy shared by constituent elements of the target depends upon the mass of the implanted ions. The energy is transferred more efficiently to the constituent element whose mass is closer to the incident ions[19].

In the case of argon bombardment, argon has a mass closer to sulfur than to cadmium and therefore transfers more energy to sulfur atoms in binary collisions. This compensates for the difference in mass effect and binding energy effect, which favour cadmium sputtering. In the same way, bismuth being closer to cadmium in mass, it transfers more energy to cadmium atoms in the binary collision and enhances the cadmium sputtering.

Kelly and Naguib's[18] theory of preferential sputtering also predicts preferential sputtering of cadmium.

5.4 Trapping of implanted ions

Results show that the number of trapped 80 keV Bi atoms saturates at $\sim 1.5\times10^{16}$ ions/cm^2 for a fluence of $\sim 4\times10^{16}$ ions/cm^2 while 40 keV Ar saturates at 2.3×10^{16} ions/cm^2 for a fluence of $\sim 6\times10^{16}$ ions/cm^2. Saturation fluences calculated from Carter[32] et al are $\sim 2\times10^{16}$ ions.cm^{-2} for 80 keV bismuth and 1.4×10^{17} ions.cm^{-2} for 40 keV argon.

Baxter[42] found a saturation fluence of 2×10^{16} ions.cm^{-2} for 40 keV bismuth and 1×10^{17} ions.cm^{-2} for 40 keV argon for single crystal CdS. These results are in good agreement with the findings of Chernow et al and Govind et al for CdS implanted with doses up to 3×10^{16} ions.cm^{-2}.

The calculated bismuth saturation fluence is about one half of that observed, while the calculated argon saturation fluence is about twice that of the observed value.

CONCLUSIONS

The following conclusions have been drawn from the results and discussion presented earlier.

(1) Thin films of CdS grew epitaxially on the (111) face of single crystal silicon. The epitaxial relations were (00.1)CdS||(111)Si; <11.0>CdS||<110>Si.

(2) The basic crystal structure did not change even with the highest fluences of Bi^+ (5×10^{16} ions/cm^2) and of Ar^+ (6.7×10^{16} ions/cm^2).

(3) Channeling results showed that the critical angle of cadmium has increased after bismuth and argon bombardment.

(4) Preferential sputtering of cadmium for 80 keV Bi^+ implantation was observed. The cadmium excess dropped by 10% for a fluence of 5×10^{16} ions/cm^2.

(5) No significant preferential sputtering was observed for 40 keV Ar^+ either at 40°K or at room temperature.

(6) Sputtering results can be explained qualitatively by considering a) the enhanced efficiency of energy transfer to that component of compound whose atomic mass is closer to implanted ions, b) the mass effect and c) the binding energy effect.

(7) Saturation trapping was observed at fluences $\sim 4\times10^{16}$ ions.cm^{-2} and $\sim 6\times10^{16}$ ions/cm^2, for 80 keV Bi^+ and 40 keV Ar^+ respectively.

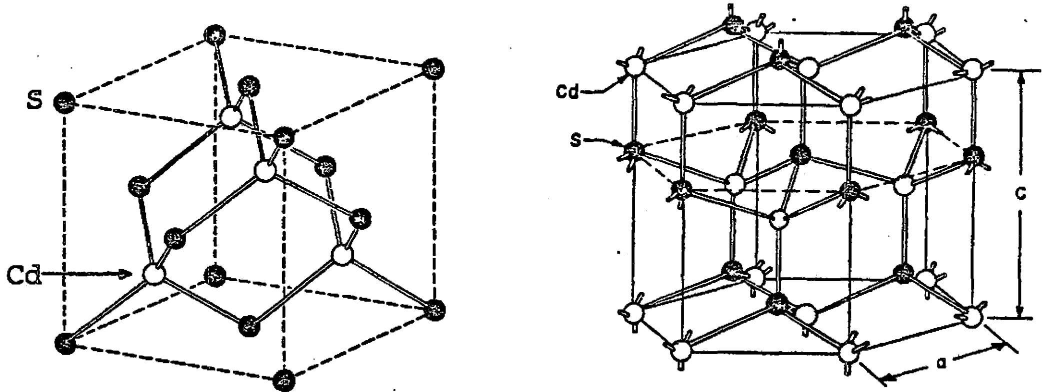

(a) Cubic zinc blende lattice (b) Hexagonal wurtzite lattice

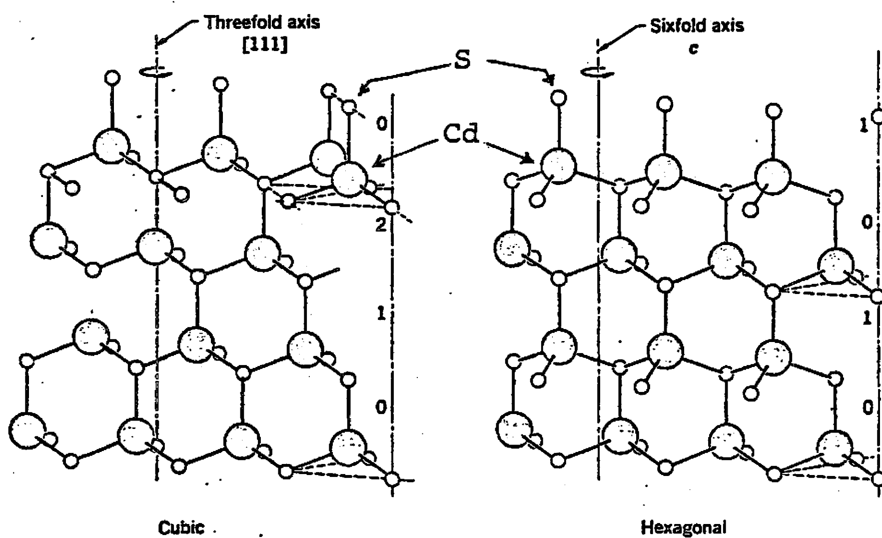

(c) Stacking of tetrahedral layers in cubic and hexagonal CdS

Fig. 1 Crystal structure of CdS

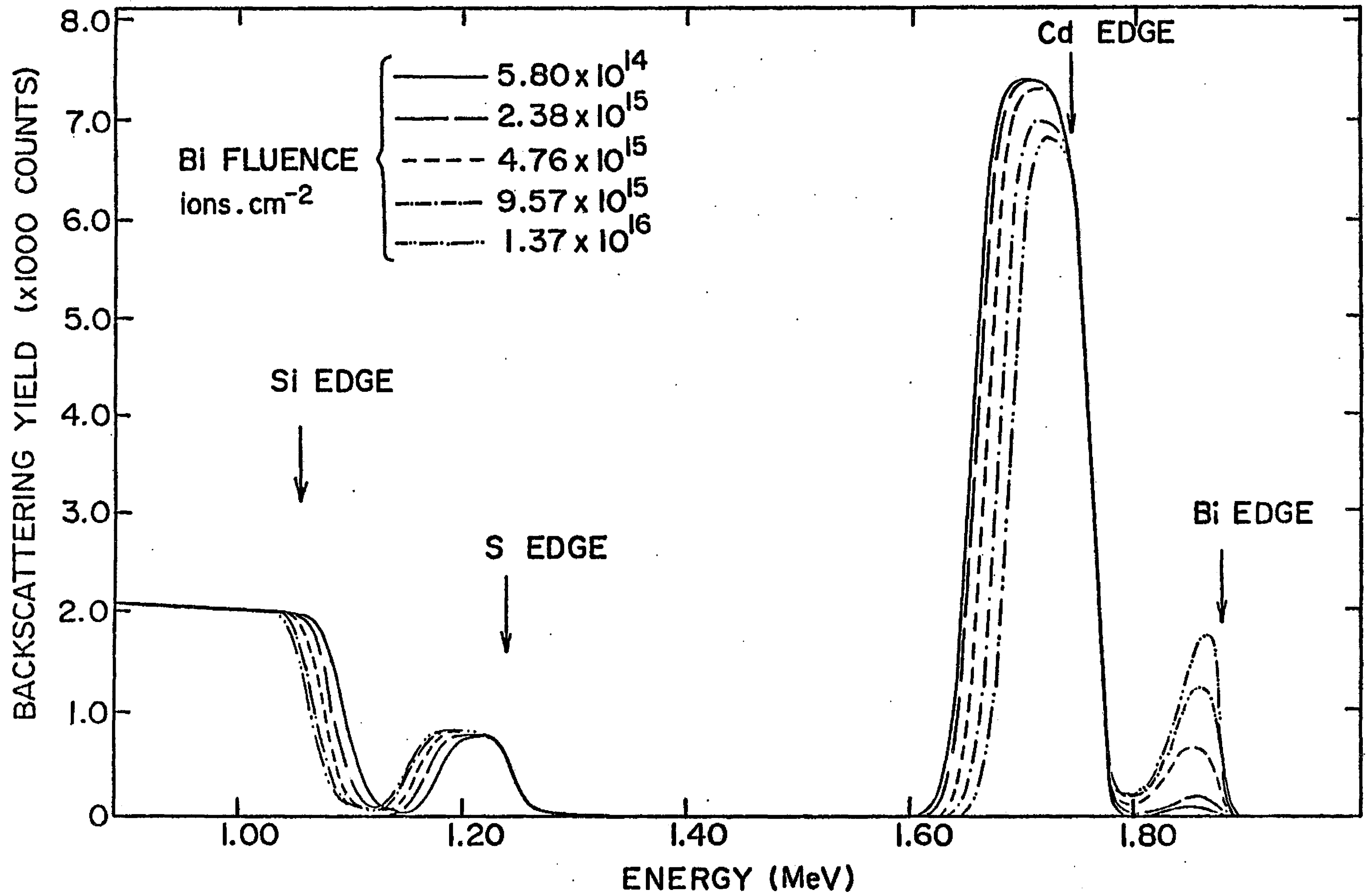

Fig. 2 RBS spectra after various fluences of Bi^{+}

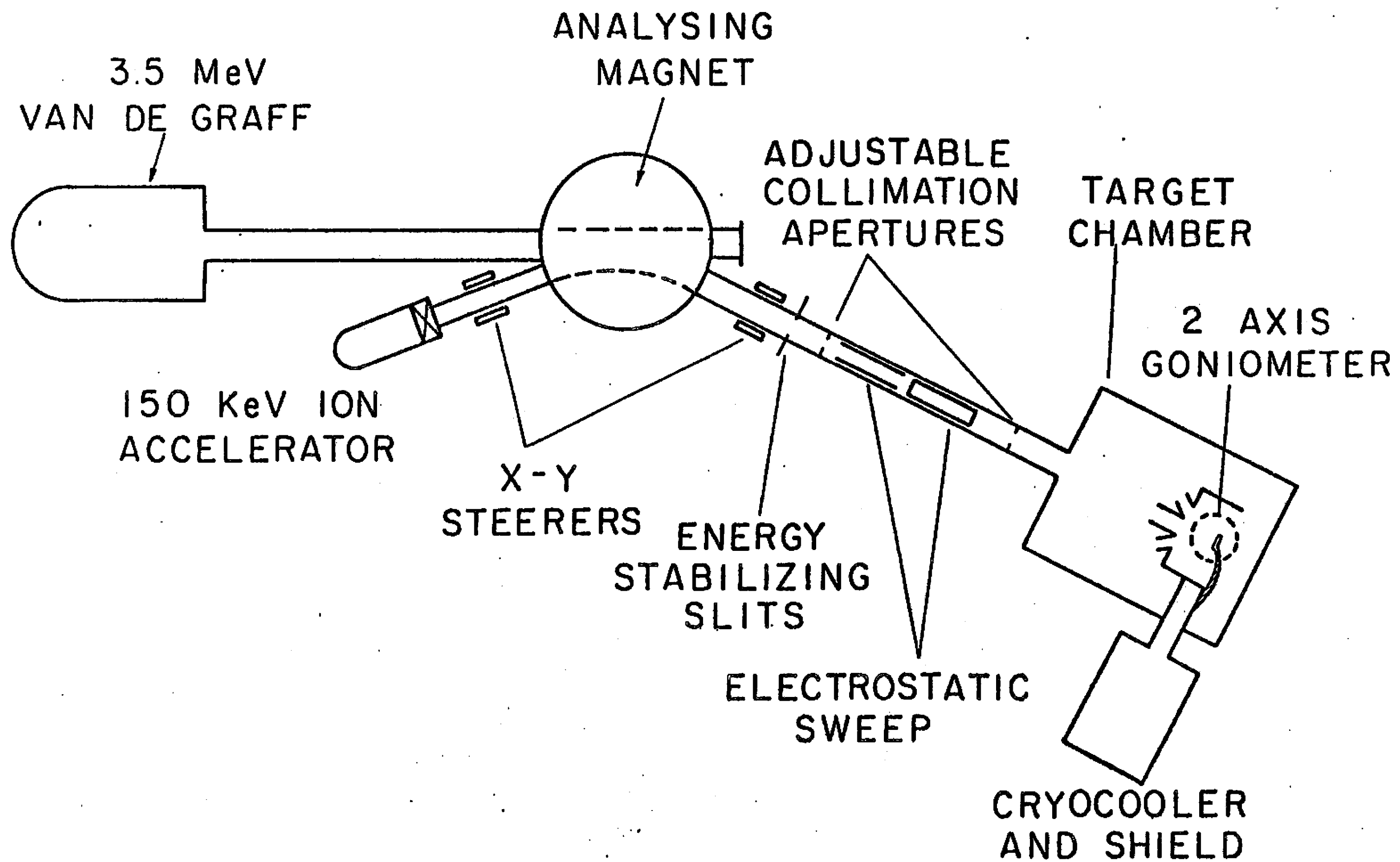

Fig. 3 Schematic of McMaster on-line RBS and ion implantation facility

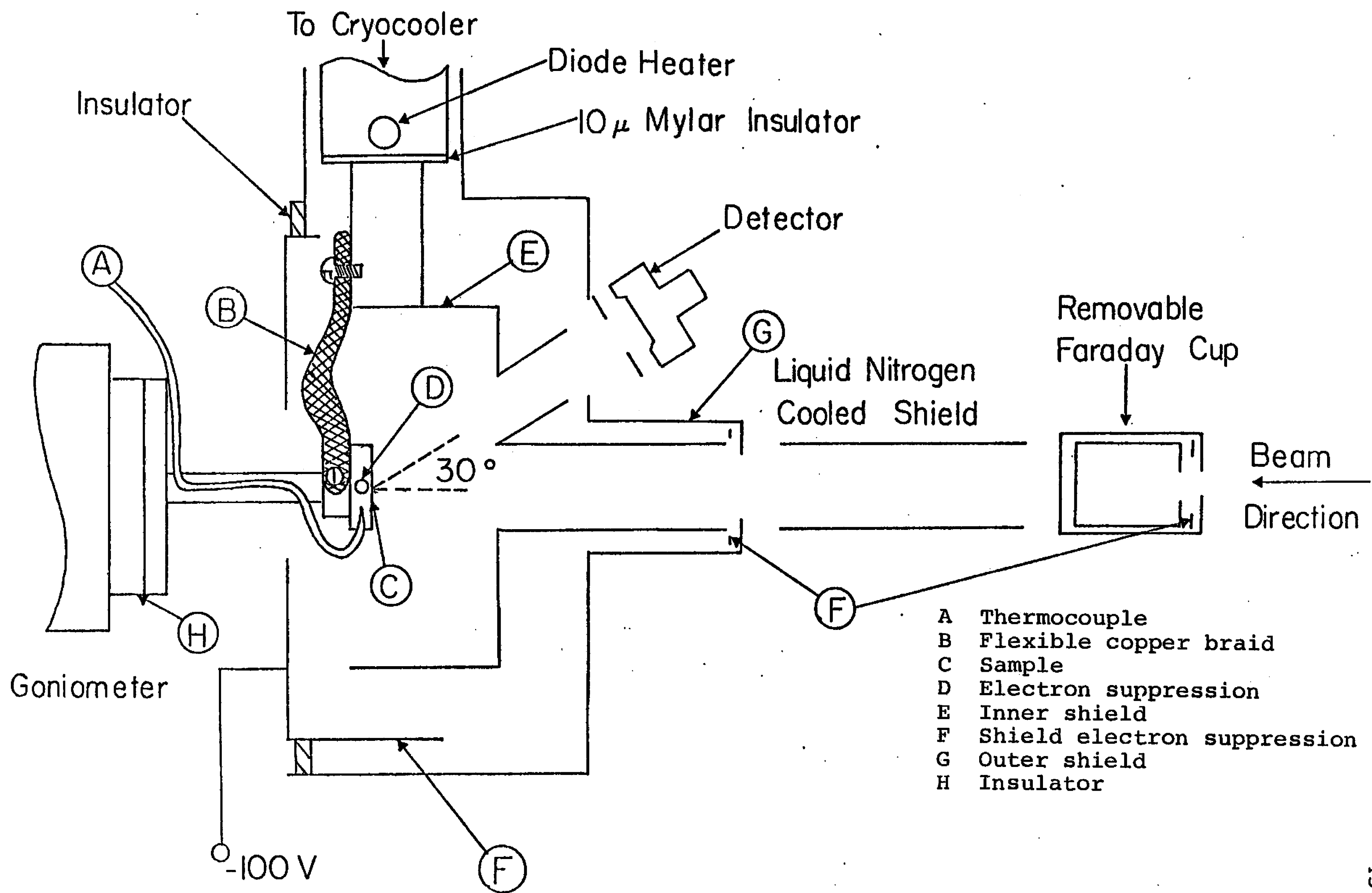

Fig. 4 A schematic of target chamber

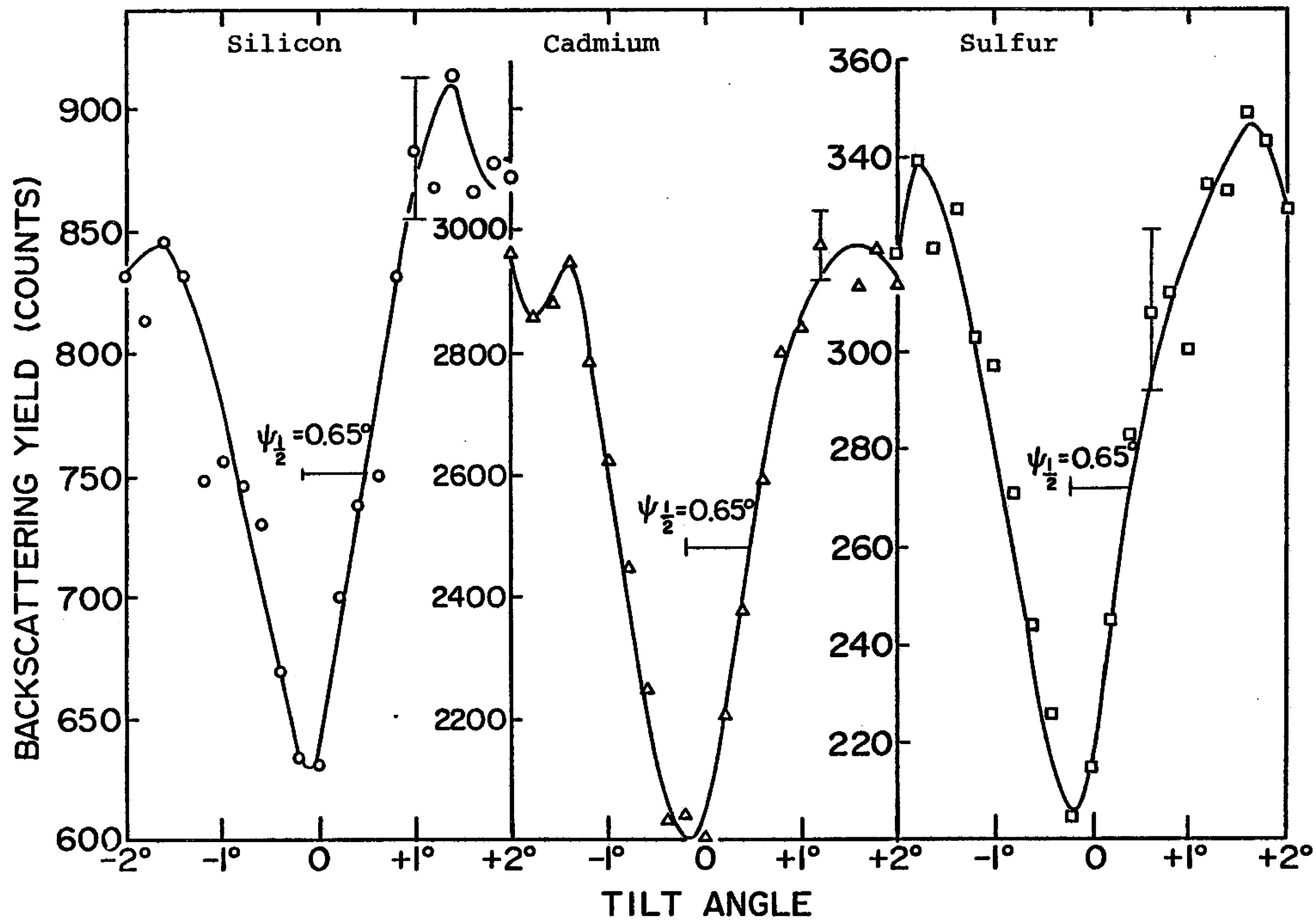

Fig. 5 Backscattering yield versus tilt angle for silicon, cadmium and sulfur (unbombarded sample)

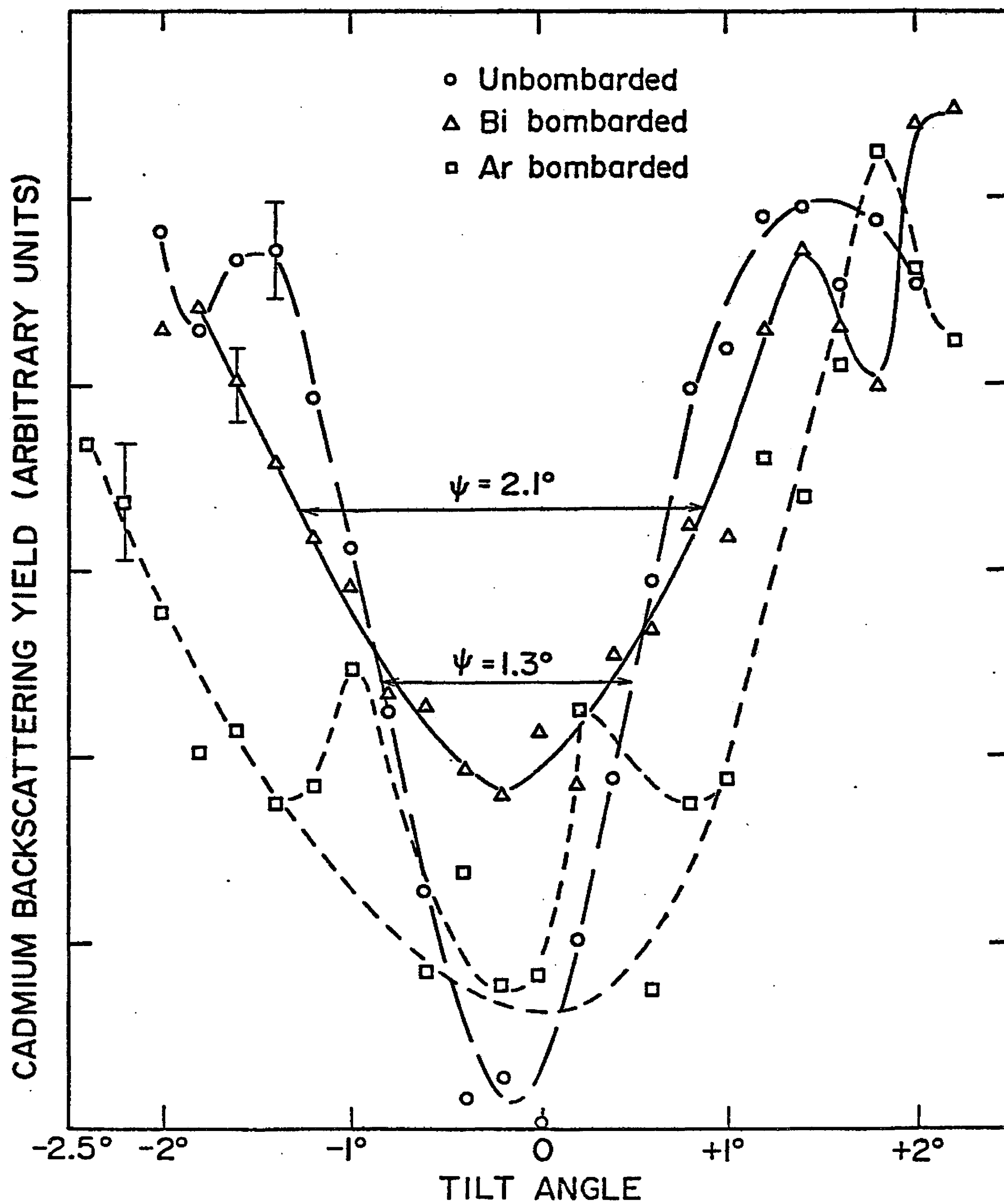

Fig. 6 Backscattering yield versus tilt angle for cadmium before and after bismuth and argon bombardment

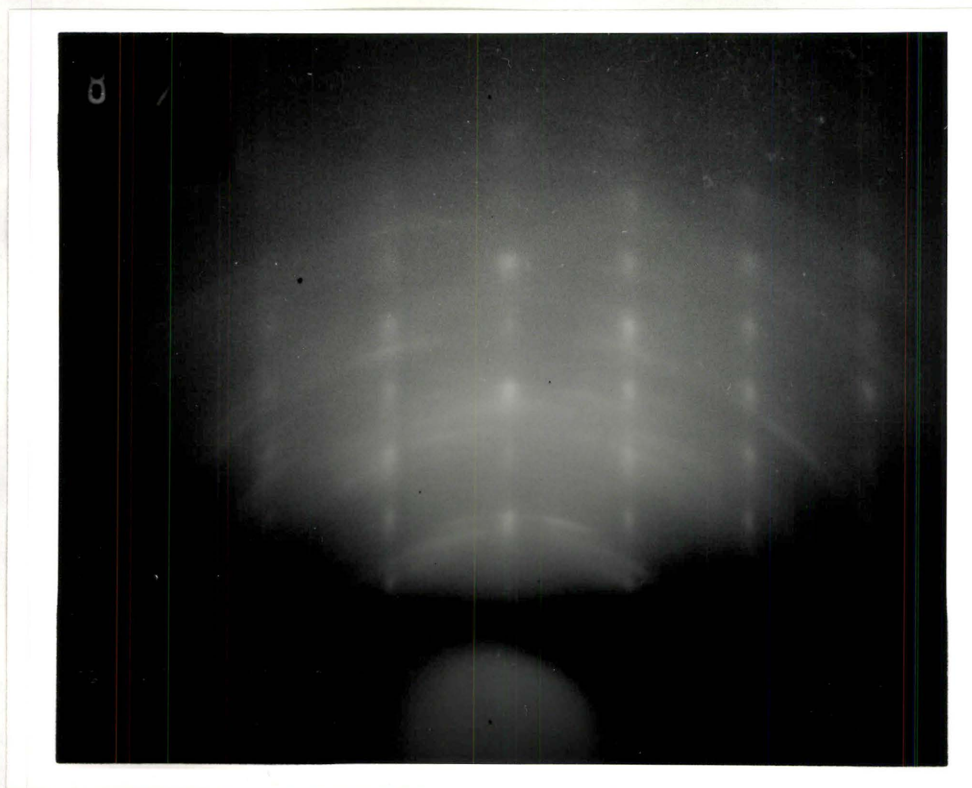

Fig. 7 A RHEED pattern from an unbombarded CdS thin film

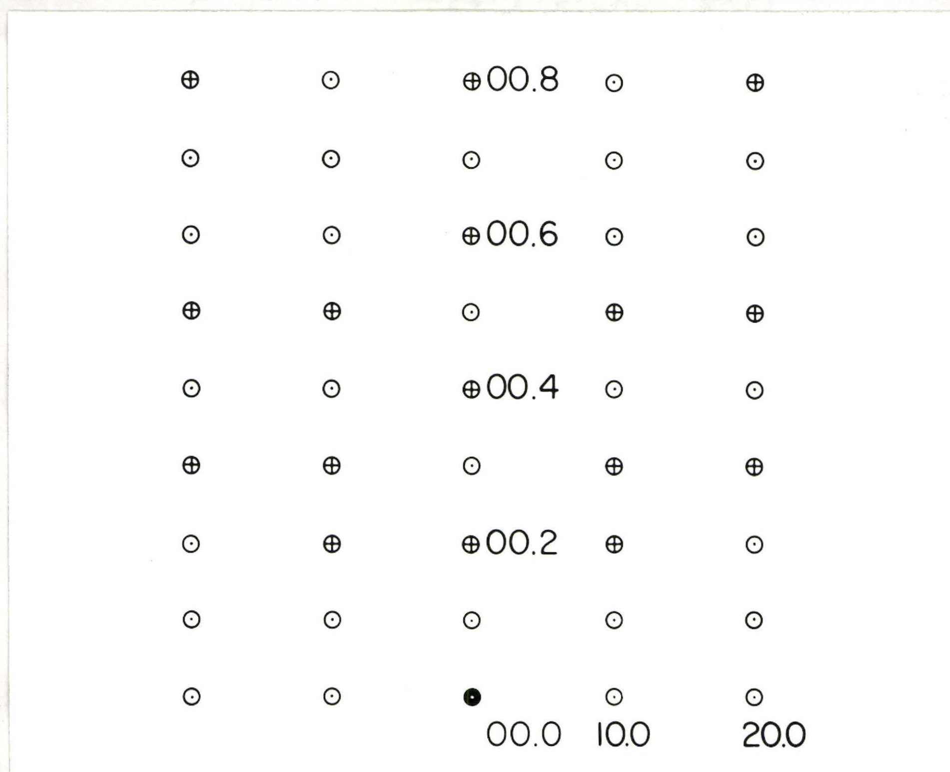

Fig. 8 A theoretical pattern corresponding to Fig. 7

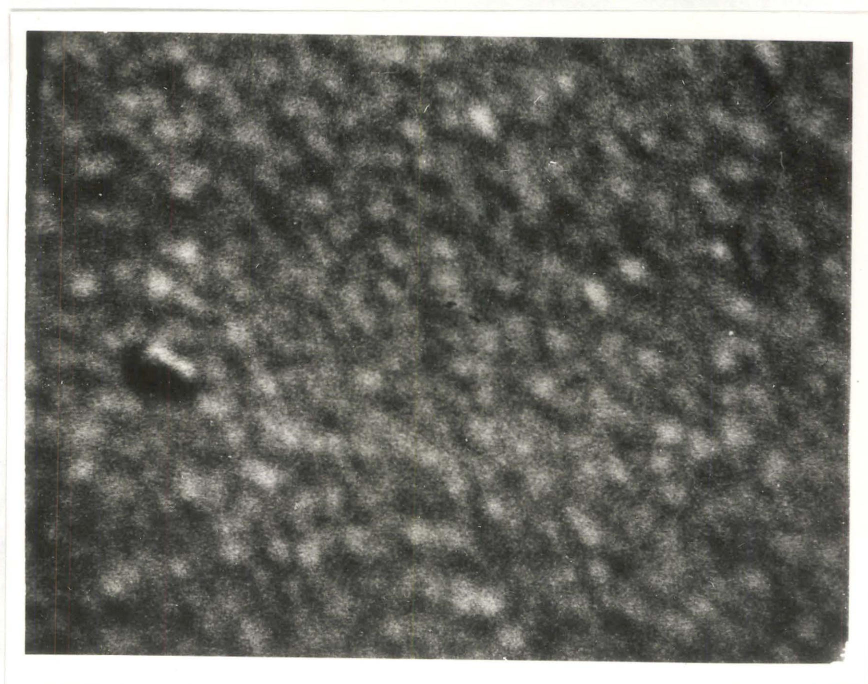

Fig. 9 An SEM microphotograph of an unbombarded CdS film

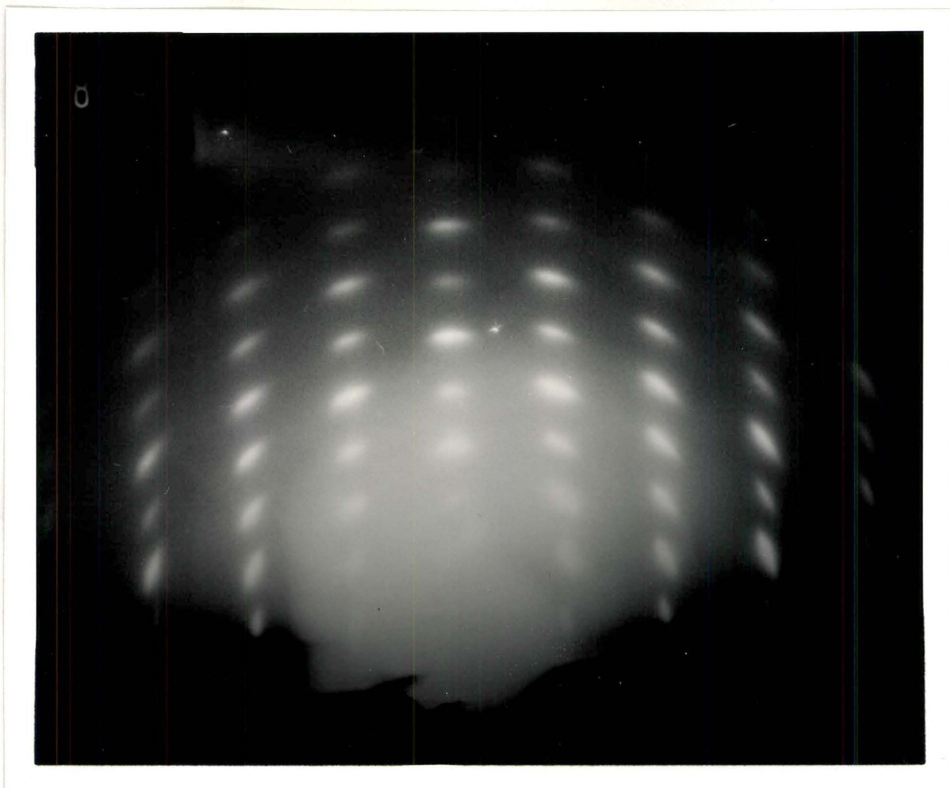

Fig. 10 A RHEED pattern from a Bi^{+} bombarded CdS film

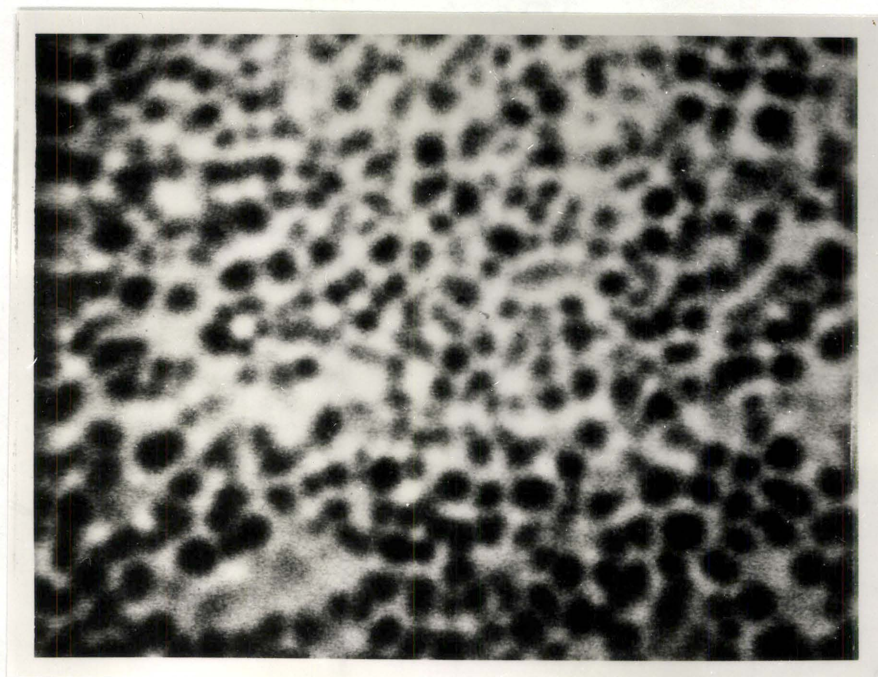

Fig. 11 An SEM microphotograph of a Bi^{+} bombarded CdS film

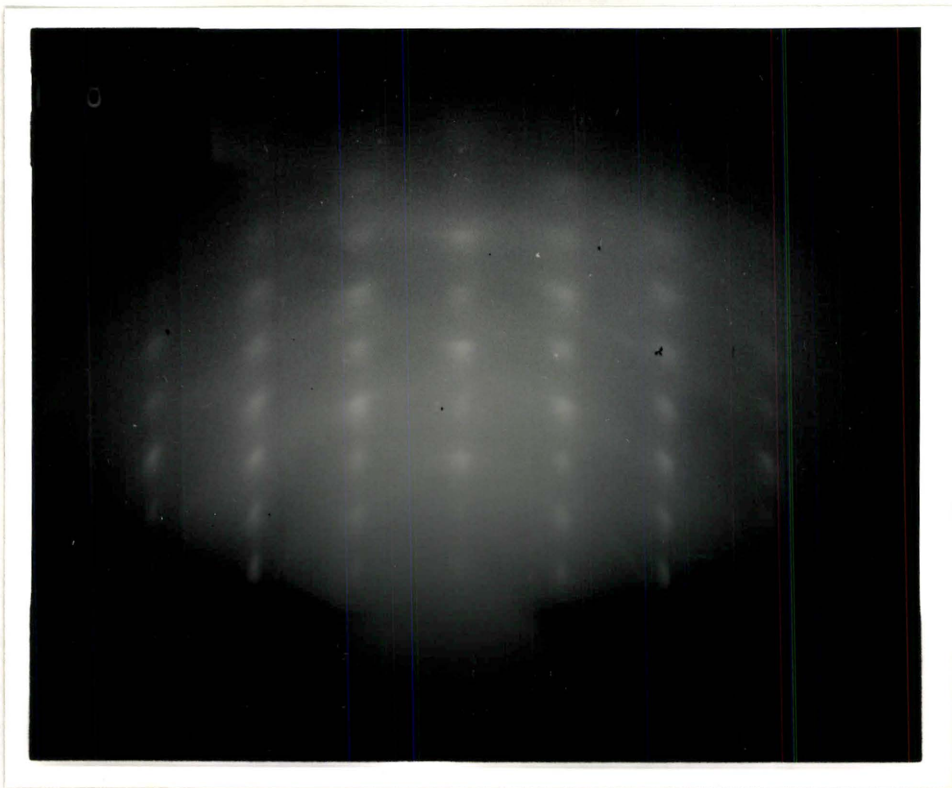

Fig. 12 A RHEED pattern from an Ar^{+} bombarded CdS film

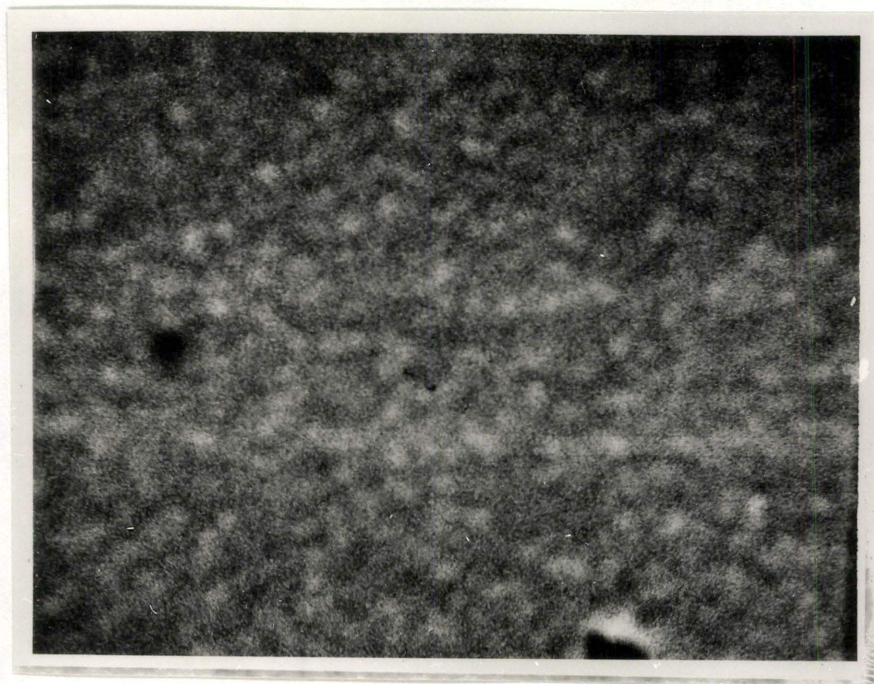

Fig. 13 An SEM microphotograph of an Ar^{+} bombarded CdS film

unbombarded

AREAL DENSITY OF Cd RETAINED ($\times 10^{17}$ atoms.cm^{-2})

AREAL DENSITY OF S RETAINED ($\times 10^{17}$ atoms.cm^{-2})

Bi$^+$ FLUENCE (atom. cm^{-2})

Fig. 14 Plot of areal density of Cd and S retained versus Bi$^+$ fluence

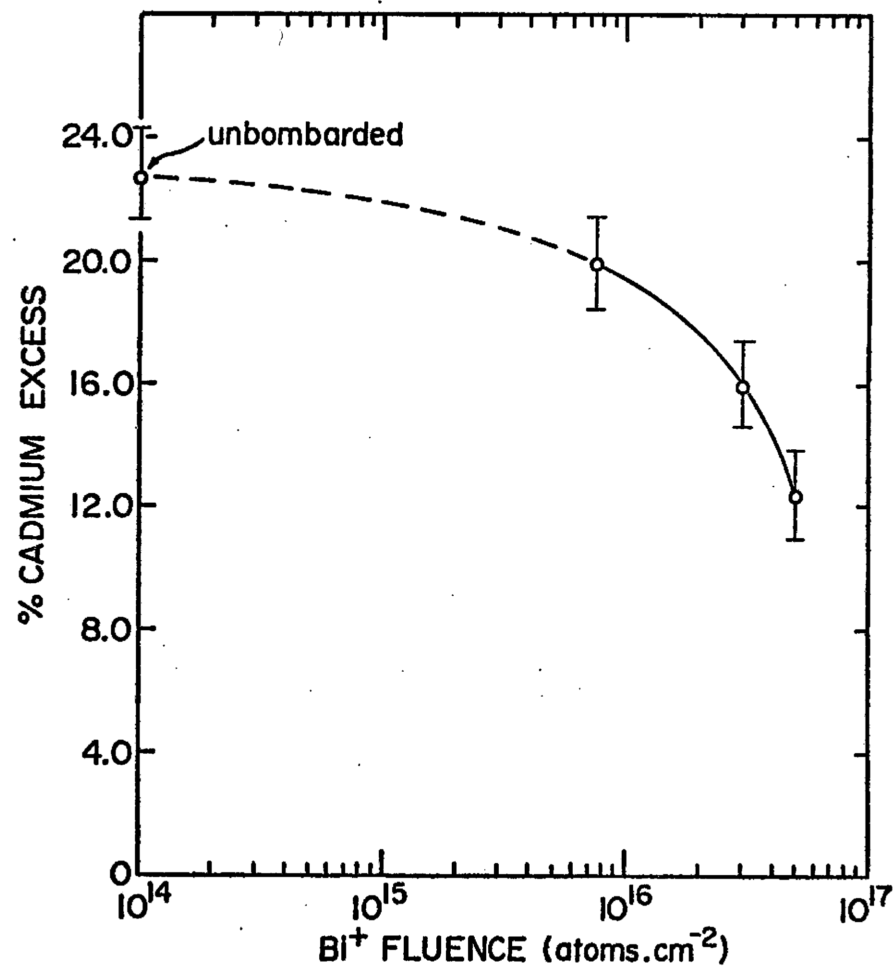

Fig. 15 Plot of percent of Cd excess w.r.t. stoichiometric compound versus Bi$^+$ fluence.

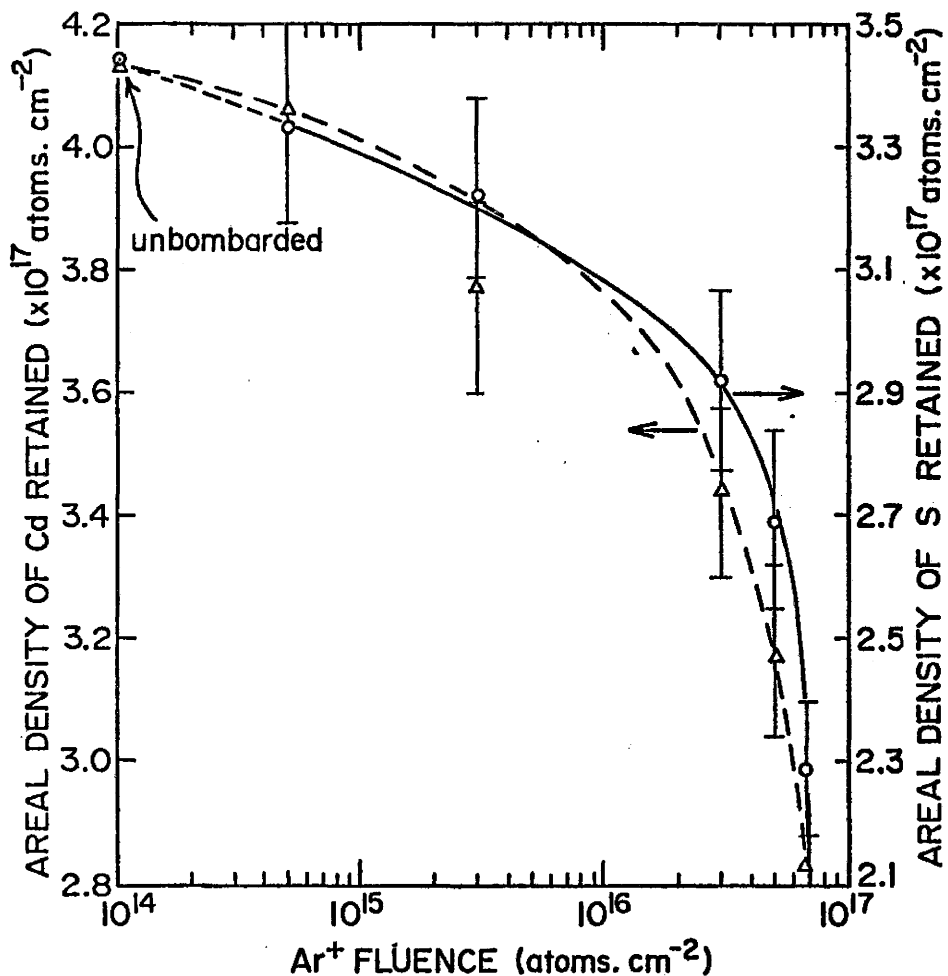

Fig. 16 Plot of areal density of Cd and S retained versus Ar^+ fluence (sample at 40°K)

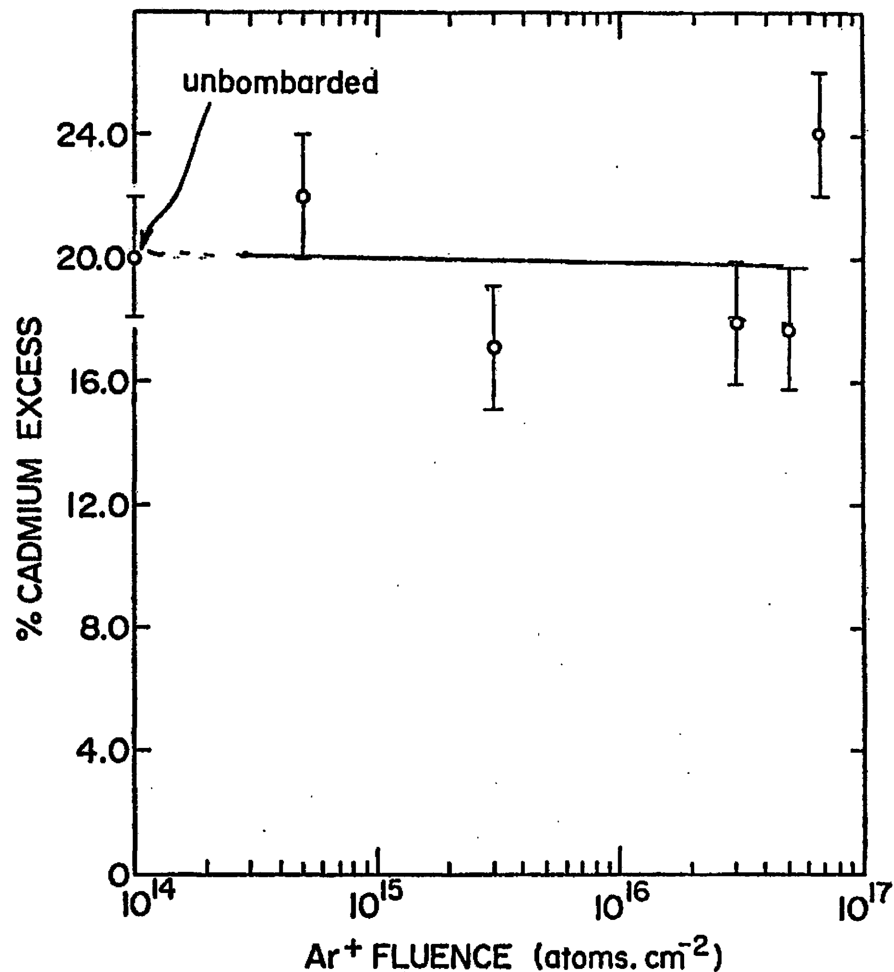

Fig. 17 Plot of percent of Cd excess w.r.t stoichiometric compound versus Ar^+ fluence

AREAL DENSITY OF Cd RETAINED ($x10^{17}$ atoms.cm^{-2})

4.4
4.0
3.6
3.2
2.8
2.4
2.0
1.6

AREAL DENSITY OF S RETAINED ($x10^{17}$ atoms.cm^{-2})

4.2
3.8
3.4
3.0
2.6
2.2
1.8
1.4
1.0

1 2 3 4 5 6 7 8 9 10

Ar^+ FLUENCE ($x10^{16}$ atoms. cm^{-2})

Fig. 18 Plot of areal density of Cd and S retained versus Ar^+ fluence (sample at 298°K)

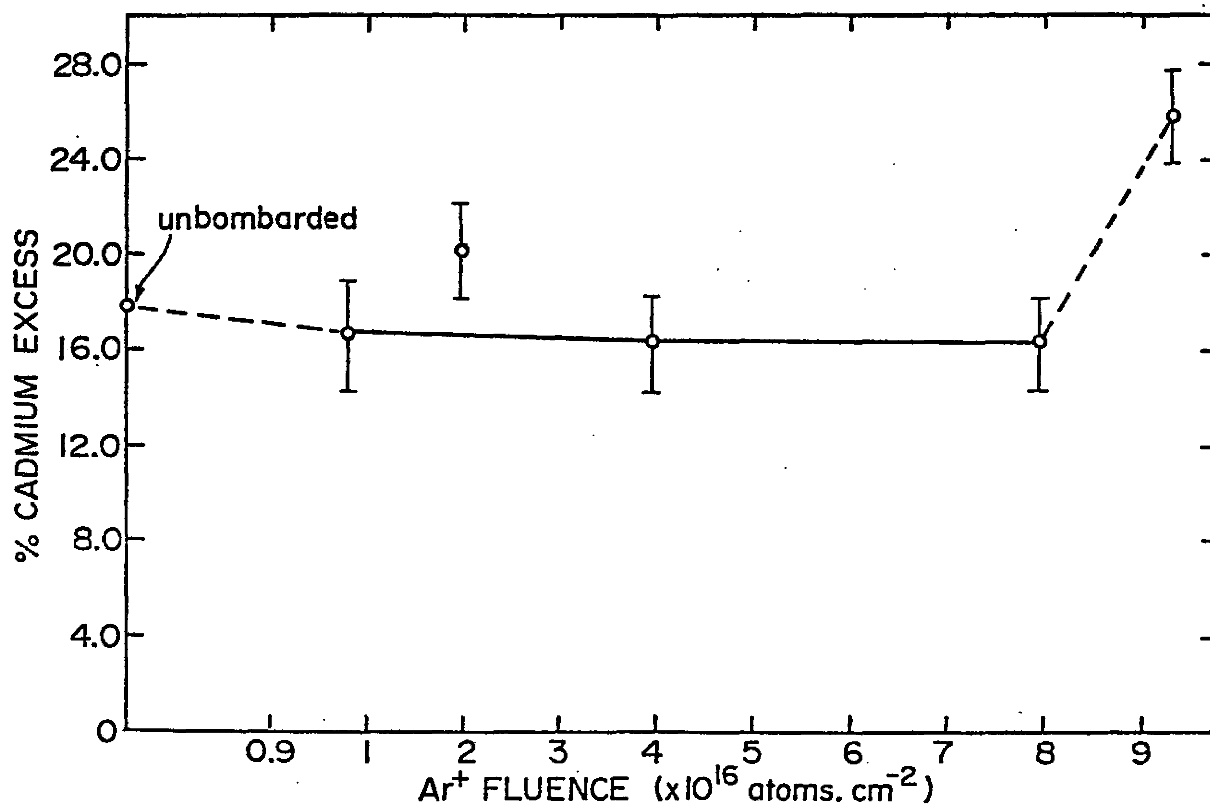

Fig. 19 Plot of percent cadmium excess w.r.t. stoichiometric compound versus Ar^+ fluence

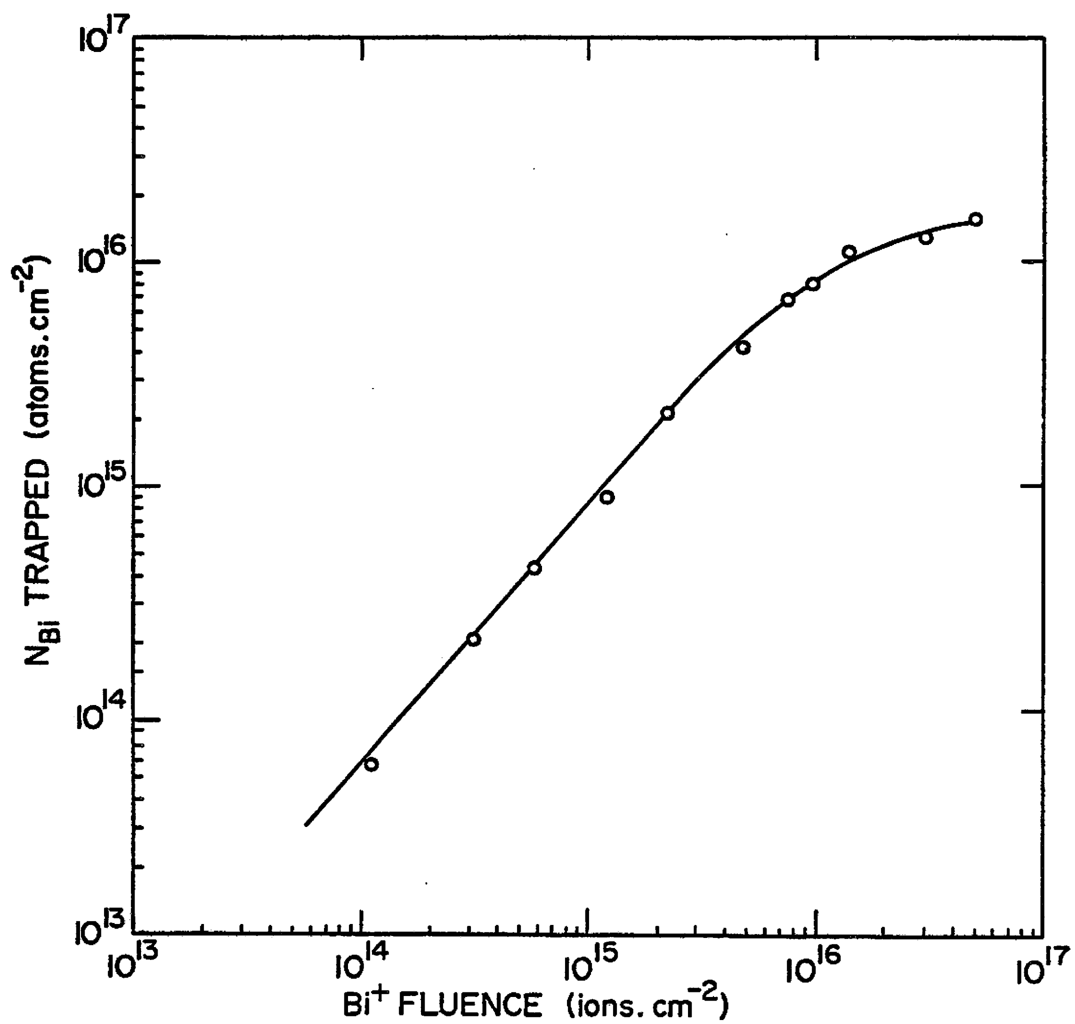

Fig.20 Plot of trapped Bi atoms versus Bi^{+} fluence

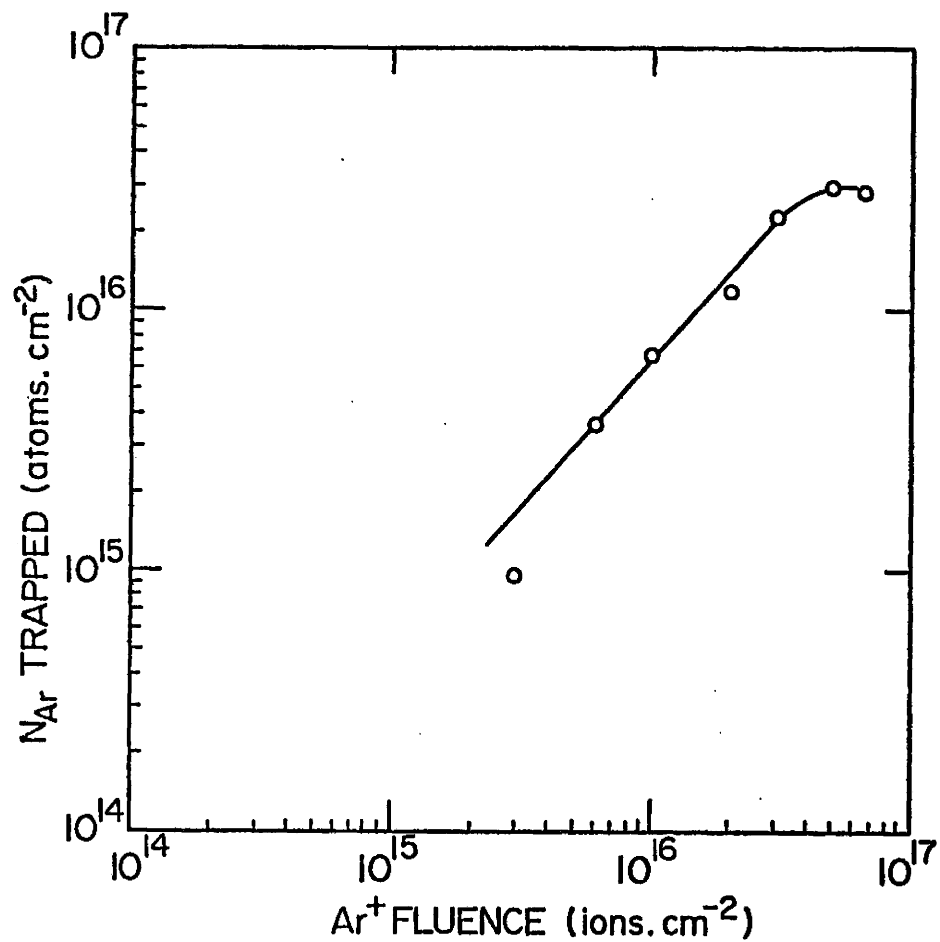

Fig. 21 Plot of trapped Ar atoms versus Ar^+ fluence (sample at 40°K)

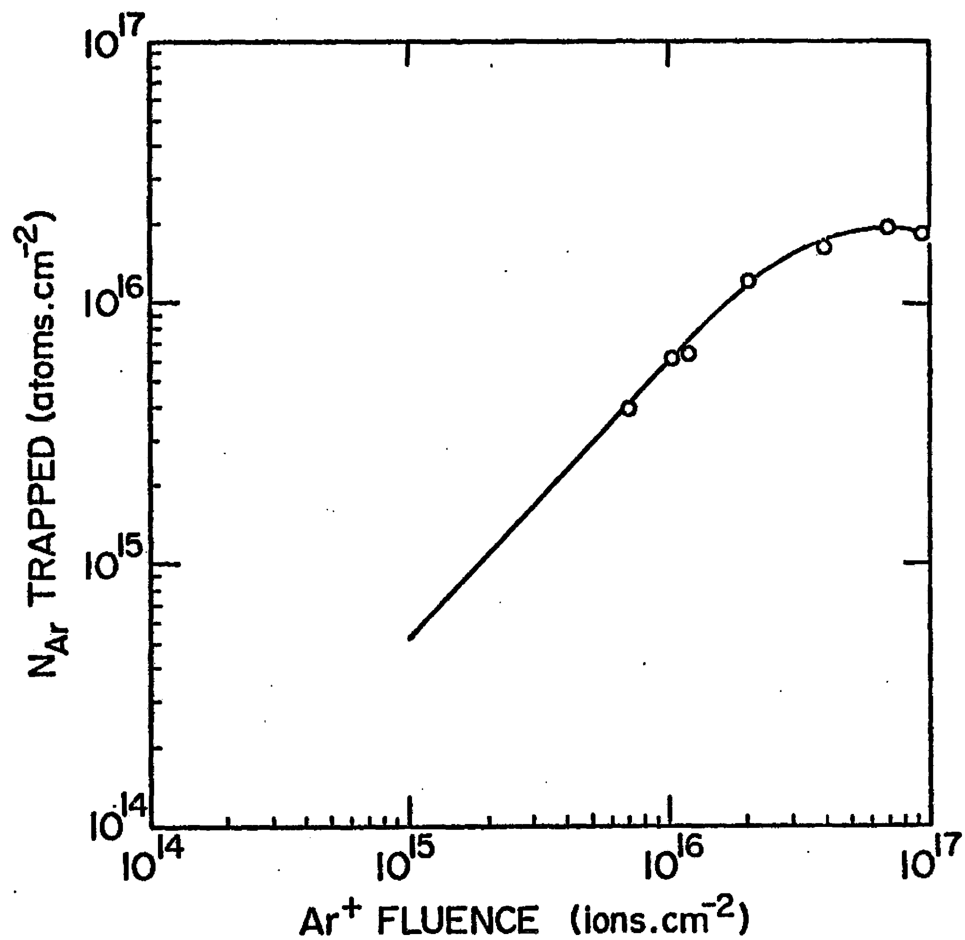

Fig. 22 Plot of trapped Ar atoms versus Ar^+ fluence (sample at 298°K)

REFERENCES

1) F. A. Kroger, J. Phys. Chem. Sol. 26 (1965) 1717.

2) W. W. Anderson and J. T. Michell, Appl. Phys. Lett. 12 (1968) 334.

3) Y. Shiraki, T. Shimada and K. F. Komastubara Proc. Third Int. Conf. on Ion Implantation in Semiconductors and Other Materials. Ed. B. L. Crowder. Pub. Plenum Press, N.Y. (1973) 395.

4) J. W. Mayer, L. Eriksson and J. A. Davies; Ion Implantation in Semiconductors, Academic Press (1970).

5) Application of Ion Beams to Materials, Eds. G. Carter, J. S. Colligon and W. A. Grant. Pub. Inst. of Physics, London (1976).

6) V. Ashworth, D. Baxter, W. A. Grant and R.P.M. Procter; Proc. Int. Conf. on Ion Implantation in Semiconductors and Other Materials, Osaka, 1974. Ed. S. Namba, Pub. Plenum Press, N.Y.

7) G. K. Wehner in Methods of Surface Analysis, Ed. A. W. Czanderna (Elsevier, New York, 1975) Chap. 1.

8) R. Kelly, Nucl. Instrum. Methods, 149 (1978) 553.

9) P.S. Ho, J.E. Lewis, H.S. Wildman and J.K. Howard, Surf. Sci. 57 (1976) 393.

10) Z.L. Liau, W. L. Brown, R. Homer, and J.M. Poate, Appl. Phys. Lett. 30 (1977) 626.

11) R. Kelly and J.B. Sanders, Nucl. Instrum. Methods 132 (1976) 335.

12) T. Parker and R. Kelly, Proc. Int. Conf. on Ion Implantation in Semiconductors and Other Materials, Ed. B.L. Crowder, Pub. Plenum Press; N.Y. (1973) 551.

13) Epitaxial Growth, Ed. J.W. Matthews. Pub. Acad. Press, New York (1975) p. 658 (Materials Science Series).

14) B. A. Kulp and R. H. Kelly, J. of Appl. Phys. 31 (1960) 1057.

15) B. A. Kulp, Phys. Rev. 159 (1967) 603.

16) M. Neuberger, Electronic properties information center, Hughes Aircraft Company, Culver City, Calif. 90230. Contract F 33615/68/C/1225.EPIC S II (1969).

17) Semiconducting II-VI, IV-VI, V-VI Compounds by N. Kh. Abrikosov, V. F. Bankina, L.V. Poretskaya, L.E. Shelimova. Plenum Press, New York, 1969.

18) H. H. Naguib and R. Kelly, Rad. Effects, 25 (1975) 1.

19) P. Sigmund, Phys. Rev. 184 (1969) 383.

20) M. Ono, Y. Takasu, K. Nakayama, and T. Yamashina, Surf. Sci. 26 (1971) 313.

21) R.R. Olson and G. K. Wehner, J. Vac. Sci. Technol. 14 (1977) 319.

22) N. Andersen and P. Sigmund, K. Dan. Vidensk, Selsk. Mat. Fys. Medd. 39 No. 3 (1974).

23) P. K. Haff, Yale Report No. 3074-422 (1977).

24) H. H. Andersen and H. L. Bay, J. Appl. Phys. 45 (1974) 953.

25) R. Kelly, Proc. Sympo on Sputt., Ed. P. Varga, G. Betz and F.P. Viehböck (Vienna, April 1980) 390.

26) H. H. Brongersma, M.J. Spornaay and T.M. Buck, Surf. Sci. 71 (1978) 657.

27) L.E. Rehn, P.R. Okamoto, D.I. Potter, and H. Wiedersich, J. Nucl. Mater. 74 (1978) 242.

28) E. Rutherford, Phil. Mag. (6) 21 (1911), 669.

29) P. Townsend, J.C. Kelly, N.E.W. Hartley, Ion Impl., Sputt., and their Appl., Academic Press (1976) 181.

30) D. S. Gemmell, Rev. Mod. Phys. 46 (1974) 129.

31) E.V. Kornelsen, Can. J. Phys. 42 (1964) 364.

32) G. Carter, J.S. Colligon and J. H. Leck, Proc. Phys. Soc. 79 (1962) 299.

33) K.B. Winterbon, Ion Implantation Range and Energy Deposition Distribution, Vol. 2, Plenum Press, New York (1975).

34) A. Lopez-Otero. Thin Solid Films 49 (1978) 3.

35) T.M. Vanderwel, M. Eng. Report, Dept. of Eng. Phys. McMaster University, April 1978.

36) R.S. Walker, Ph.D. Thesis (1977), Dept. of Electrical Engineering, McMaster University, Hamilton, Ont.

37) P.B. Hirsch, A. Howie, R.B. Nicholson, D.W. Pashley and M.J. Whelan, Electron Microscopy of Thin Crystals (Butterworths, London, 1967), p. 141.

38) N.G. Dhere and N.R. Parikh, J. Vac. Sci. & Technol. 13 (1980) 714.

39) D.A. Thompson, A. Golanski, K.H. Haugen, D. Stevanovic, G. Carter and C.E. Cristodoulides, Rad. Eff. 80 (1980) 69.

40) P.K. Govind and F.J. Fraikor, J. Appl. Phys. 42 (1971) 2476.

41) G. Eldridge, P.K. Govind, D.A. Nieman, and F. Chernow; Proc. of European Conf. on Ion Implantation, University of Reading (Peter Peregrinus, Harts, U.K., 1970) 143.

42) D. Baxter, Ph.D. Thesis, Dept. of Electrical Engineering, Univ. of Salford, England (1977).